Short-wave infrared (SWIR) spectral and geochemical characteristics of hydrothermal alteration at the Archean Izok Lake Zn-Cu-Pb-Ag volcanogenic massive sulfide deposit, Nunavut, Canada: application in exploration target vectoring

K. Laakso[a*†], J.M. Peter[b], B. Rivard[a], and H.P. White[c]

[a]Centre for Earth Observation Sciences, Department of Earth and Atmospheric Sciences, University of Alberta, 1-26 Earth Sciences Building, University of Alberta, Edmonton, Alberta, Canada, T6G 2E3
†present address: Specim Ltd., Elektroniikkatie 13, FI-90590 Oulu, Finland
[b]Geological Survey of Canada, 601 Booth Street, Ottawa, Ontario, Canada, K1A 0E8
[c]Canada Centre for Mapping and Earth Observation, Natural Resources Canada, 560 Rochester Street, Ontario, Canada, K1A 0E4

[*]Corresponding author. Tel.: +358-40-732-6672; E-mail: kati.laakso@iki.fi

January 10th 2016

Abstract: Short-wave infrared (SWIR) field and laboratory spectra were used to identify and characterize hydrothermal alteration mineral chemical variability in host rocks proximal to the Izok Lake Zn-Cu-Pb-Ag volcanogenic massive sulfide (VMS) deposit in Nunavut, Canada. The deposit is hosted within a sequence of predominantly felsic pyroclastic rocks of Archean age that are regionally metamorphosed to amphibolite facies. These rocks are characterized by the muscovite-biotite-sillimanite and chlorite-biotite-cordierite mineral suite. Proximal to the deposit white micas are Al-rich to potassic muscovite, and the biotite and chlorite are Mg-rich. In areas that are immediately outboard of the proximal alteration zones, rocks are altered to Al-poor muscovite and intermediate to Fe-rich biotite and chlorite. Outboard of this, distal areas are characterized by potassic muscovite and Mg-rich biotite and chlorite. The white micas and biotite/chlorite group minerals display considerable variation in their Al-OH and Fe-OH absorption feature wavelength positions. The variations in muscovite and biotite/chlorite compositions (as determined by the Al-OH and Fe-OH absorption feature wavelength positions) broadly correlate with changes in hydrothermal alteration intensity, as measured by the Ishikawa and chlorite-carbonate-pyrite alteration indices. Our findings suggest that the large-scale alteration intensity trends of the Izok Lake study area can be elucidated using the spectral properties of the hydrothermal alteration minerals.

1. Introduction

Volcanogenic massive sulfide (VMS) deposits form in submarine tectonic settings characterized by rifting and high heat flow that initiate hydrothermal circulation of seawater through rock strata in the subsurface (Galley et al., 2007). The processes by which the host rocks to VMS deposits are altered are reasonably well constrained, based on theoretical and experimental studies on ancient and modern deposit studies (e.g.,

Large, 1977; Seyfried et al., 1988; Gemmell and Large, 1992; Galley, 1993; Goodfellow and Peter, 1994; Ohmoto, 1996). Prior to VMS deposit formation, cold seawater is drawn into the upper parts of the crust, heated and a convective cell of circulating hydrothermal fluids is created. As the fluid temperature increases and pH concomitantly decreases, metals are leached from the host rocks by the hydrothermal fluids. The dissolved metals are transported upward and precipitated at or near the seafloor where the hydrothermal fluids mix with cold seawater. A key geochemical reaction along the fluid flow path is the breakdown of feldspars through interactions with the acidic hydrothermal fluids, and the subsequent formation of white micas and chlorite (Barrett and MacLean, 1994). Herein, white mica refers to dioctahedral phyllosilicate minerals that display a solid solution between paragonite-muscovite and muscovite-phengite (Velde, 1965). Many VMS systems (i.e., the entire footprint of the deposit, including subtle textural, geochemical, mineralogical, and mineral chemical features imparted on the host rocks) have two distinct alteration styles: 1) primarily chlorite-altered, typically centered on the core of the fluid upflow zone, and 2) sericite-altered, typically peripheral to the chlorite-altered zone (Barrett and MacLean, 1994).

Although the most intense hydrothermal alteration (forming at high temperatures of 300-400 $^{\circ}$C and high water/rock ratios; Barrett and MacLean, 1994) is commonly manifest within the core of the hydrothermal upflow zone, peripheral to mineralization, alteration effects are more subtle (less intense), and their recognition can aid in vectoring toward mineralization in an exploration program. Vectoring methods include the quantification of the enrichment and depletion of particular elements, such as (expressed as oxides) Na_2O, CaO and K_2O (Stephens et al., 1984). Bulk rock sodium depletion is documented in the vicinity of most VMS deposits (Franklin, 1997), and several studies (see Franklin et al., 1975 and references therein) have mapped the spatial variability of this depletion as a proxy for alteration intensity variability throughout a study area.

Alteration indices, such as the commonly used Ishikawa alteration index (hereafter referred to as AI; Ishikawa et al., 1976) and the chlorite-carbonate-pyrite index (CCPI; Large et al., 2001), offer a more sophisticated method of quantifying alteration intensity by tracking multiple geochemical and mineralogical parameters. The AI measures the depletion (Na_2O and CaO) and enrichment (MgO and K_2O) of alkaline earth and alkali metal oxides associated with the formation of white mica and chlorite. One disadvantage of the use of the AI is that it does not consider carbonate alteration, which can be significant in some VMS deposits (Large et al., 2001). Consequently the chlorite-carbonate-pyrite index (CCPI) is used in the present study to measure the abundance of chlorite through FeO and MgO enrichment and Na_2O and K_2O depletion. Both the AI and the CCPI range between 0 and 100%, such that the maximum value represents complete replacement of feldspar and volcanic glass by white micas, chlorite, or both.

Conventional methods of determining the chemical compositions of rocks and minerals (e.g., whole rock and electron microprobe analysis, respectively) can be time-consuming and costly. A rapid and non-destructive alternative to these methods is optical remote sensing. Many phyllosilicate minerals are infrared-active, and can be identified using their characteristic absorption features in the short-wave infrared (SWIR) wavelength region. More specifically, muscovite has a pronounced Al-OH absorption feature near 2200 nm, and chlorite group minerals have an Fe-OH absorption feature near 2260 nm (Hunt and Salisbury, 1970). The Fe-OH absorption feature is also present in biotite in the same wavelength region (Post and Noble, 1993). Like chlorite, biotite can form either during regional metamorphism or hydrothermal metasomatism (Pirajno, 2009). The wavelength position of these absorption features shifts as a function of compositional changes that take place in response to changing chemical and temperature gradients within a VMS system. High temperatures favor a decrease in the Mg and Fe content and an increase in the Al content of white mica (Duke, 1994).

Moreover, the Fe contents of chlorite and biotite can increase with formation at higher temperatures (Miyashiro and Shido, 1985; Cathelineau, 1988). Additionally, other factors such as pressure, hydrothermal fluid chemistry, water/rock ratios and the composition of the host rocks can all simultaneously influence the chemical composition of the phyllosilicate minerals (Kranidiotis and MacLean, 1987). The compositional changes that take place as a result of these processes are manifested in the wavelength position of the Al-OH absorption feature, which shifts toward shorter wavelengths as the Al content of the octahedral sites of the mineral increase, and the opposite effect, or a shift toward longer wavelengths when the Mg and Fe contents of the octahedral sites increase (Post and Noble, 1993; Duke, 1994). Similarly, the hydroxyl absorption features of biotite and chlorite shift toward shorter wavelengths with increasing Mg, and toward longer wavelengths with increasing Fe (Bassett, 1960; McLeod et al., 1987).

In a prior publication (Laakso et al. 2015) we examined the application of large-scale airborne hyperspectral imagery to detect hydrothermal alteration zones in the Izok Lake Zn-Cu-Pb-Ag VMS deposit, Nunavut, Canada, one of the largest undeveloped Zn-Cu deposits in North America (Morrison, 2004). We first documented the links between the position of key spectral features (Fe-OH, Al-OH) of constituent phyllosilicate minerals (biotite, chlorite and white mica) in altered rhyolites and the chemistry of these minerals using petrographic and mineral chemistry data. From the analysis of ground hyperspectral results we then revealed a systematic trend in the Fe-OH absorption feature wavelength position of biotite/chlorite with distance from the VMS deposit. A spatial pattern of relatively long Al-OH absorption feature wavelength positions was also observed in the vicinity of Izok Lake using ground and airborne hyperspectral sensors. This area coincides with relatively long Fe-OH absorption feature positions, detected by means of ground spectra. These findings showed that hydrothermal alteration zones could be detected by hyperspectral remote sensing, despite the presence

of abundant lichen cover in the study area.

In the present study we have investigated the relationship between bulk rock compositions and the spectral properties of the constituent phyllosilicate minerals in the hydrothermal alteration zones of the Izok Lake deposit, with the aim of developing methodologies that can be used to vector toward concealed mineralization here and elsewhere. The present investigation extends the previous study by Laakso et al. (2015) by linking hydrothermal alteration intensity metrics, extracted from lithogeochemical data, to hyperspectral data obtained from rock outcrops and drill cores of the Izok Lake deposit. These lithogeochemical and spectral data are used to define the fine-scale spatial distribution of the alteration trends in the study area.

2. Study Area

Izok Lake (65°38'N, 112°48'W; Fig. 1) is a Zn-Cu-Pb-Ag VMS deposit located in the Kitikmeot region of Nunavut, Canada. The total resource presently is 14.4 million tonnes grading 2.52% Cu, 12.94% Zn and 71 g/t Ag (MMG Ltd., 2011). The Izok Lake deposit is hosted within the Point Lake Formation, a succession of felsic and mafic metavolcanic rocks that belong to the Yellowknife Supergroup of the Slave Structural Province.

The deposit comprises five polymetallic, texturally and mineralogically complex massive to semi-massive lenses of sphalerite, pyrite, chalcopyrite and galena hosted by Archean (2.6 Ga) rhyolitic rocks that are regionally metamorphosed to middle amphibolite facies (Bostock, 1980; Mortensen et al., 1988; Morrison, 2004). The presence of the assemblage anthophyllite-cordierite-spinel-corundum, the porphyroblastic textures and widespread occurrence of sillimanite collectively indicate that the metamorphic conditions may have reached peak temperatures of 700 °C and pressures of between 0.2 and 0.3 GPa in the vicinity of mineralization (Morrison, 2004).

The rocks of the study area have undergone three phases of deformation (Morrison, 2004). The first phase is evidenced as a pervasive, planar fabric parallel to bedding. The second phase is expressed as crenulation cleavage and lineation in the northern parts of the study area. The massive sulfide lenses are located in the middle of an antiform that may (in part) be a primary volcanic domal structure and (in part) a structure induced by the third phase of deformation (Morrison, 2004).

Immediately adjacent to a set of southwest trending faults the rocks have been hydrothermally altered in an asymmetric fashion (Fig. 1). The known mineralization is located underneath Izok Lake in five massive sulfide lenses (North, Northwest, Central - West, Central - East and Inukshuk) shown in Figure 2. The hanging wall and footwall host felsic volcanic rocks are visually and geochemically very similar to each other and are in places intensely altered (Morrison, 2004). The timing of hydrothermal alteration is syn-volcanic and syn-mineralization (Morrison, 2004), and, therefore, our spectral measurements and geochemical data are focused exclusively on the hydrothermally altered rhyolitic rocks. This hydrothermal alteration is manifest by an inner core of chlorite-rich rocks that is surrounded by a broad zone of sericite-rich rocks (Morrison, 2004). The inner alteration zone is characterized by Mg-enriched rocks comprised mainly of chlorite, biotite and cordierite (Money and Heslop, 1976). The immediate hangingwall rocks (predominantly rhyolite; andesite in some places) are sodium-depleted and contain widespread muscovite, biotite and sillimanite (Morrison, 2004). Nowak (2012) interpreted muscovite and biotite to be the peak metamorphic products of the precursor syn-volcanic hydrothermal alteration minerals white mica and chlorite, respectively. The lack of a exhalitive sediments lateral to the deposit, the primary presence of stringer mineralization lateral to the massive sulfide lenses, and the presence of intense alteration in the hanging wall to the deposit were among the factors that led Morrison (2004) to suggest that the deposit formed through sub-seafloor mineralization

processes.

The syn-volcanic and syn-mineralization hydrothermal alteration is overprinted by younger calcic metasomatism, which is evidenced by a wide range of CaO contents in the rhyolitic rocks spanning from trace amounts to over 11 wt% (Morrison, 2004). Nowak (2012) attributed the variation in the CaO content of the rhyolitic rocks of the study area to variable dissolution of feldspar during hydrothermal alteration. However, the timing and significance of this calcic metasomatism are currently not well understood.

3. Sampling and Methods

3.1 Outcrop spectra site selection and measurement

The surface expression of the hydrothermally altered rocks was delineated by collecting 455 spectral measurements and 60 samples (Fig. 1) from rhyolite outcrops during summer 2010 and 2013. The area of most intense alteration extends approximately 4.7 km west from the known mineralization (Fig. 1), and hence the outcrop spectral measurements collected farther away from the mineralization are likely from rocks that are the least altered or weakly altered in the study area. Nevertheless, all the spectral measurements are included in the data analysis to obtain a complete understanding of the spectral features and trends throughout the study area. The rationale for site selection (and further description of data acquisition to that given below) is provided in Laakso et al. (2015).

All measurements were obtained using a PANalytical (formerly ASD, Inc., Boulder, CO) FieldSpec Pro® (abbreviated hereafter as "ASD") 3 spectrometer that records spectra in the 350-2500 nm wavelength range with a spectral resolution of 10 nm and a sampling interval of 1 nm in the short-wave infrared (SWIR; 1300-3000 nm) wavelength region. The spectrometer was connected to a contact probe that has an

internal illumination source that ensures consistent illumination conditions during data acquisition. The raw at-sensor radiance values were converted to surface reflectance values by means of a Spectralon™ reflectance panel (i.e. the "white reference", SRT-99-100, Labsphere, Inc., North Sutton, NH, USA), a commercially available plate made of polytetrafluoroethylene (Bruegge et al., 1993). Finally, these relative reflectance values were converted to absolute reflectance values by multiplying the relative reflectance value of each wavelength with the reflectance factor obtained from the calibration certificate of the Spectralon™ panel, in accordance with the procedure of Clark et al. (2002).

3.2 Drill core sampling and laboratory spectral measurements

In order to establish the character and extent of the hydrothermal alteration zones of the Izok Lake deposit in the subsurface, spectroscopic data were obtained from 28 drill cores (Figs. 1-2). These measurements were made with PANalytical TerraSpec® 4 Hi-Res and ASD spectrometers at an average down-hole spacing of 5.5 m, resulting in 781 spectral readings from all lithologies intersected in the drillholes. As with the outcrop spectral measurements, the drill core spectra were acquired using a contact probe. The TerraSpec4 spectrometer acquires data with a spectral resolution of 6 nm and sampling interval of 1 nm in the SWIR wavelength region. Each spectrum acquired from the drill cores consists of 60 individual measurements taken consecutively and averaged by the instrument. Conversion of radiance to reflectance was as described for outcrop spectral measurements and only the drill core spectra that were acquired from the rhyolite samples were analyzed.

In addition to acquiring spectral measurements, a visual estimate of the hydrothermal alteration intensity at each spectral measurement area was recorded for a subset of eight drill cores (HEN-172, HEN173, HEN-197, HEN-198, HEN-212, HEN-

273, HEN-309 and HEN-340) that collectively comprise a cross-section through a Central - West massive sulfide lens. For this subset, each spectral measurement has an associated alteration intensity that ranges from weak, to moderate, to intense, based on the textural and mineralogical properties of the rock. These were then assigned visually estimated alteration intensity (VEAI) values, with 1 indicating weak alteration, 2 representing moderate alteration, and 3 representing intense alteration. The examined drill core profiles do not show visible signs of weathering that could potentially affect the interpretations of the spectral measurements.

3.3 Laboratory spectral and spatial analysis

Of the 781 spectra acquired from the drill cores, 624 are from rhyolitic rocks and these were investigated to delineate the vertical extent of hydrothermal alteration and document any zonation present. In the case of the outcrop spectrometry, 50 of the 455 spectral measurements were discarded because of low signal-to-noise ratios. The remaining 405 spectra and the 624 drill core spectra were hull-corrected (continuum-removed) to minimize the effects of background absorption (Clark, 1999), and the hull quotient minima of the Al-OH and Fe-OH absorption features were estimated manually. Visualization of the spatial trends of the outcrop spectroscopic Al-OH and Fe-OH absorption feature wavelength positions was done by interpolation by Kriging (Oliver and Webster, 1990) using the nearest 10 values to calculate the contents of each pixel in the continuous surface. The results were spatially restricted to the outcrop limits of the rhyolitic rocks in the study area.

In a separate analysis, the Euclidean distance between the Al-OH and Fe-OH absorption feature observations of the drill cores and their spatially nearest massive sulfide lenses was calculated to investigate possible changes in the spectral properties of

the white micas and biotite/chlorite with distance to the mineralization. The locations and spatial dimensions of the massive sulfide lenses were extracted from the drill core logs of MMG Ltd. In the case of outcrop spectra, the distance between the measurement locations and the nearest subcropping or subsurface massive sulfide lens (see Figure 1) was calculated. Finally, all measured distances were combined to construct a three-dimensional model of the spatial variation of the Al-OH and Fe-OH absorption feature wavelength positions.

3.4 Bulk geochemical analytical techniques

A database of whole rock major element oxide analyses of 2902 rock samples collected from outcrops at an average sample spacing of 43 m was provided by MMG Ltd. These samples are from outcrops of intensely altered rocks proximal to mineralization and outcrops of less altered rocks distal to mineralization. This database was supplemented by a similar bulk compositional database of 151 drill core samples (NQ core, 4.5 cm diameter, each 15 to 20 cm long) collected at 28 m intervals down-hole. The drill core samples are mainly from intensely altered rocks proximal to mineralization. The locations of the surface samples and drill cores are shown in Figure 1.

For the whole rock major element oxide analyses, the samples were crushed, split and powdered using a hardened steel mill. Powdered samples (0.2 g) were added to a lithium metaborate and lithium tetraborate flux (0.9 g), mixed and fused in a furnace at 1000 °C. The samples were then cooled and dissolved in 100 mL of 4% nitric acid/2% hydrochloric acid. This solution was analyzed by Inductively Coupled Plasma-Atomic Emission Spectroscopy (ICP-AES). The results were corrected for spectral inter-element interferences. Oxide abundances were calculated from the determined elemental

contents with 0.01% and 100% lower and upper limits, respectively.

3.5 Lithogeochemical data treatment (AI, CCPI, & VEAI analyses)

The outcrop lithogeochemical data were used to identify large-scale variations in the intensity and style of hydrothermal alteration across the study area. First, the outcrop samples were restricted to rhyolite (shown in Figure 1) and the Nb, Y, Zr and TiO_2 values of the remaining 555 lithogeochemical analyses were used to classify the volcanic rocks in the study area. This was conducted by means of the Winchester-Floyd diagram (Winchester and Floyd, 1977) that is used to differentiate rock types based on their characteristic proportions of the minor and trace elements that are relatively immobile during the alteration of the volcanic rocks. This analysis was only conducted using the outcrop lithogeochemical data because the drill core lithogeochemical database lacks the requisite immobile element data.

The alteration intensity variation throughout the study area was further assessed by calculating the Ishikawa index (AI, Ishikawa et al., 1976):

$$AI = 100(K_2O + MgO)/(K_2O + MgO + Na_2O + CaO).$$

The AI values were spatially linked to corresponding outcrop spectral measurements of the rhyolitic rocks to investigate the relationship between the Al-OH and Fe-OH wavelength positions and intensity of hydrothermal alteration. This was achieved by horizontally linking each Al-OH and Fe-OH absorption feature in the outcrop spectra with the AI value calculated from its geographically nearest lithogeochemical analysis. The AI was used as a measure of alteration intensity due to the predominantly white mica-rich nature of the rhyolitic rocks surrounding the massive sulfide lenses. The alteration intensity variation throughout the study area was further

investigated by calculating the chlorite-carbonate-pyrite index (CCPI) using the following equation (Large et al., 2001):

$$CCPI = 100(FeO + MgO)/(FeO + MgO + K_2O + Na_2O).$$

The CCPI is a measure of chlorite replacement of white micas and feldspar group minerals. The AI and CCPI values of the study area were then plotted into an alteration box plot (Large et al., 2001) to assist in distinguishing different alteration trends in the study area.

In order to explore the relationships between the Al-OH and Fe-OH absorption features and alteration intensity in a vertical (depth) sense, 122 drill core whole rock analyses of the rhyolitic rocks were correlated with their nearest Al-OH and Fe-OH absorption features in the drill core spectra. The alteration intensity was estimated by means of the AI and the CCPI. The AI and CCPI alteration index values (n=122) were then combined with their spatially nearest VEAI values (n=172). Only VEAI values for the rhyolitic rock units were included in this analysis. No VEAI value was assigned to an AI or CCPI value for down-hole distances between the AI, CCPI and the VEAI values of greater than five meters.

The AI and CCPI values were then compared with the Al-OH and Fe-OH absorption features for the drill core rhyolitic rocks with the objective of associating the wavelength position shifts with the vertical hydrothermal alteration intensity variation. Due to the different sampling intervals of the analytical and spectral results, the latter were linearly interpolated to the nearest whole rock geochemical analysis. The Al-OH and Fe-OH absorption feature wavelength positions situated immediately down-hole and up-hole from the geochemical analysis were used to calculate the interpolated Al-OH and Fe-OH absorption feature wavelengths. If interpolation was not possible due to a missing value either below or above a particular geochemical analysis, no extrapolation

was performed, and the analysis was not assigned a corresponding Al-OH and Fe-OH absorption feature wavelength value. This resulted in 112 Al-OH values and 97 Fe-OH values that were spatially combined with their nearest rock geochemical analysis. Correlations were not assigned for drill cores HEN-258, HEN-418 and HEN-444 due to a lack of geochemical data.

Finally, the Kriging interpolation technique (Oliver and Webster, 1990) was used to map and visualize the spatial distribution of the alteration intensity values throughout the study area. The nearest 10 alteration intensity values, estimated by means of the AI, were used to calculate the content of each pixel in the interpolation surface. In this analysis, all the outcrop lithogeochemical samples that lie within the surface spatial limits of the rhyolitic rocks were used (n=1136) in order to estimate the alteration intensity variation throughout the study area using a maximum number of observations. For the same reason, the vertical alteration index values of the drill core database were combined with the horizontal alteration index values extracted from the surface samples. This analysis was constrained to the vertical alteration index values from a maximum depth of 10 m so that the vertical AI values are comparable with the horizontal AI values. Here, the AI was used to estimate the hydrothermal alteration intensity both vertically and horizontally, such that outcrop and drill core results could be compared. Eight AI values of the drill cores HEN-172, HEN-173, HEN-192, HEN-198, HEN-234, HEN-252, HEN-356 and HEN-400 are used in this analysis because there are lithogeochemical data for them in the chosen depth range (~2-10 m).

3.6 Mineralogy and mineral chemistry

The relationships between the Al-OH and Fe-OH absorption features and the minerals present in the samples were studied by petrographic analysis of six polished

thin sections (PTS) using a Nikon Labophot2® transmitted polarizing light microscope. The samples were selected based on the presence of an Al-OH or Fe-OH absorption feature, or both, and the presence or absence of biotite, chlorite and muscovite was recorded at over 500 random spots within each PTS (Laakso et al., 2015).

The electron probe microanalyses (EPMA) of seven PTS were conducted in order to investigate the relationship between the Al-OH and Fe-OH absorption feature wavelength shifts and the compositions of muscovite, biotite and chlorite. The samples were selected for EPMA based on the short, intermediate and long wavelength positions of their Al-OH and Fe-OH absorption features. The PTS were carbon-coated and analyzed using a JEOL 8230® electron microprobe. Mineral formulae were calculated on the basis of 22 oxygens for micas (white micas and biotite) and 28 oxygens for chlorite. The mineral cation compositions were then compared to the average Al-OH and Fe-OH absorption feature wavelength positions of the same samples from which the PTS were prepared (Laakso et al., 2015).

4. Results

4.1 Frequency distribution of Al-OH and Fe-OH absorption features

The Al-OH and Fe-OH absorption features of the outcrop and drill core datasets show a wide range of wavelength positions suggestive of considerable chemical compositional variation within the phyllosilicate minerals. This variation is discussed below in the context of the proximal (0-500 m), intermediate (500-2400 m) and distal (5700-6800 m) positions of these zones from mineralization.

Based on the petrographic analysis of the thin sections, the Al-OH absorption features are associated with the white micas and the Fe-OH absorption features are

associated with biotite/chlorite (Laakso et al., 2015). Furthermore, the EPMA results indicate that the Al-OH absorption features of the white micas shift toward shorter wavelengths with increasing Al content, and toward longer wavelengths with increasing Fe+Mg content (Fig. 3; Laakso et al., 2015). Similarly, the Fe-OH absorption features of biotite/chlorite shift toward shorter wavelengths with an increasing content octahedral Mg, and toward longer wavelengths with an increasing octahedral Fe content (Fig. 3).

The summary statistical properties (minimum, maximum, median and mode) of the outcrop and drill core datasets (Table 1) were calculated with the objective of identifying differences in the Al-OH and Fe-OH absorption feature wavelength positions of these datasets. The Al-OH and Fe-OH absorption feature wavelength position frequency distributions show that both the mode and median of the Al-OH and Fe-OH absorption feature wavelength positions are at shorter wavelengths in the drill core spectral dataset than in the outcrop spectral dataset (Fig. 4). This indicates that the chemical properties of the phyllosilicate minerals of these datasets may not be identical. Moreover, the wavelength ranges of the Al-OH and Fe-OH absorptions are wider for the drill core spectra than the outcrop spectra.

The frequency distributions of the Al-OH and Fe-OH absorption feature wavelengths were compared to the normal distribution using the Shapiro-Wilk test (Shapiro and Wilk, 1965). This test reveals that the Al-OH and Fe-OH wavelength positions of the outcrop and drill core spectra are not normally distributed (p=0). The non-normal data distributions of the outcrop and drill core spectral datasets are also expressed as asymmetry in the frequency distributions of the data sets, which are all positively skewed (Fig. 4). All data sets, with the exception of the outcrop spectra Fe-OH absorption feature wavelengths, have outliers that are more than three standard deviations from the sample mean. The skewed data distributions and the presence of outliers in the data sets necessitated the use of non-parametric statistical methods,

specifically Spearman's rank correlation analysis (rather than Pearson's) for determining the relationships between the spectral and lithogeochemical datasets, discussed in sections 4.3 and 4.4.

4.2 Evaluation of geochemical indicators of alteration intensity of the drillcore dataset

Bivariate plots of the visually estimated alteration intensity (VEAI) of the drill cores versus the calculated alteration indices CCPI and AI indicate that there is a statistically significant (Spearman's rho=0.494, n=24, p=0.14, 95% confidence level, one-tailed) correlation between the CCPI and the VEAI; however, there is no statistically significant correlation between the AI and the VEAI (Figs. 5A,B). Correlations between the VEAI and the AI and CCPI values were calculated using the Spearman's rank correlation coefficient due to the non-normal distributions of all three data sets, together with their small sample size (<30). These results suggest that the CCPI shows systematic variation with the visually observable alteration intensity parameters (textural and mineralogical) of the drill cores, whereas the AI does not. Hence the CCPI was chosen (over the AI) to assess the relationship between the alteration intensity and the Al-OH and Fe-OH wavelength positions of the drill core samples.

4.3 Relationships between drill core spectral and geochemical indicators

A comparison between the CCPI and the Al-OH/Fe-OH absorption feature wavelengths of the drill cores (Fig. 6A,B) shows a weak negative correlation (Spearman's rho=-0.333, n=112, p=0, 99% confidence level, two-tailed) between the wavelengths of the Al-OH absorption features and the CCPI and a weak positive correlation between wavelengths of the Fe-OH absorption feature and the CCPI (Spearman's rho=0.252, n=97, p=0.013, 95% confidence level, two-tailed). The average

distance between the spectral and lithogeochemical data positions is 2.9 m for the Al-OH absorption feature wavelength positions and 3.2 m for the Fe-OH wavelength positions.

The vertical alteration intensity variation was examined further by selecting seven drill cores (HEN-172, HEN-173, HEN-197, HEN-262, HEN-273, HEN-309 and HEN-340) that lie along a NW-SE trending section (Fig. 7A). The drill holes were cored in the immediate vicinity of the Central - West lens, which has the highest overall grade of the massive sulfide lenses (Morrison, 2004). The drill holes define a vertical section through this massive sulfide body that extends to a maximum depth of ≈150 m below surface and dips steeply toward the north. The cross-section encompasses predominantly rhyolitic rock units that surround and are crosscut by massive sulfides and intermediate to mafic dykes, respectively (Fig 7B).

Subsurface interpolated data from cores (Figs. 7A,B) show that the highest Zn and Cu values (Cu shown in Figure 7C) are located between 100 and 150 meters below the surface. The complexly zoned areas are characterized by high (80-96%) CCPI values in the immediate vicinity of the Cu-rich massive sulfide lens that gradually decrease to lower CCPI values (46-60%) toward the surface (Fig. 7D). However, there is small-scale spatial variation in these alteration intensity values such that the areas below the massive sulfide lenses also show very weak alteration. The results also illustrate the inverse correlation between the CCPI values and the Al-OH absorption feature wavelength positions (Fig. 7E). The correlation between the spatial distribution of the CCPI and the Fe-OH absorption feature wavelength positions is not as apparent in the respective cross section (Fig. 7F).

4.4 Relationships between outcrop spectral and geochemical indicators

A discriminant plot of incompatible element ratios indicates that most lithogeochemical samples are rhyolitic in composition (Fig. 8). Specifically, 88% of the samples are classified as rhyolite, 6% rhyodacite-dacite, 3% comendite-pantellerite, 2% andesite and 1% as andesite-basalt. Alkali basalt, sub-alkaline basalt, trachyandesite and trachyte each comprise less than 1% of the total number of lithogeochemical samples. Furthermore, the alteration box plot (Fig. 9) suggests that rhyolitic and rhyodacitic-dacitic samples encompass different alteration intensities that are distributed relatively evenly across the plot, but these samples are not in general associated with high CCPI values. In contrast, alkali basalts, andesite, andesite-basalt and sub-alkaline basalt are in general associated with high CCPI values and relatively low AI values. Comendite-pantellerite compositions are commonly associated with high AI values, and relatively low CCPI values. The paucity of trachyte and trachyandesite samples precludes determination of their hydrothermal alteration trends in the study area. It is notable that 87% of the samples are located in the "hydrothermal alteration" field in the plot, indicating that most samples are hydrothermally altered.

The relationship between the bulk rock compositional and spectral data was assessed by comparing the AI values with the Al-OH and Fe-OH absorption feature wavelength positions of the outcrop spectra. Here, the AI was used as a measure of alteration intensity due to the predominantly sericitic alteration of the rhyolitic rocks surrounding the massive sulfide lenses.

The average distance between the outcrop spectral measurements and the nearest lithogeochemical sample site is 46 m in the case of the Al-OH absorption feature measurements and 55 m in the case of the Fe-OH absorption feature measurements. Furthermore, both the Al-OH and Fe-OH absorption feature datasets have a minimum distance of 1.3 m and a maximum distance of 382 m to their nearest lithogeochemical

analysis. In the case of the Al-OH absorption feature wavelength positions, 7 samples are comendite-pantellerite (peralkaline rhyolites), 3 are rhyodacite-dacite, and 347 are rhyolite. In the case of the Fe-OH absorption feature wavelength position measurements, 4 nearest lithogeochemical samples are comendite-pantellerite and 260 are rhyolite.

The Spearman rank correlation analysis suggests that there is no statistically significant relationship between the Al-OH absorption feature wavelength positions and AI (Fig. 10A). In contrast, there is a positive correlation between the Fe-OH absorption feature wavelength positions and the AI (Spearman's rho=0.220, n=264, p=0, 99% confidence level, two-tailed, Fig. 10B). This correlation indicates that intense alteration is associated with a shift toward longer Fe-OH absorption feature wavelength positions in the outcrop spectral dataset.

4.5 Regional map patterns of the Al-OH and Fe-OH absorption feature positions

The spatial distributions of the Al-OH and Fe-OH absorption feature wavelength positions extracted from the outcrop spectra display spectral shifts with distance to mineralization. The intermediate areas (500–2400m) display relatively long Al-OH and Fe-OH wavelength positions (Figs. 11A,B) that correlate with relatively high to moderate AI values in the areas proximal (and intermediate) to the massive sulfide lenses (Fig. 11C).

The spatial distributions of the Al-OH and Fe-OH absorption feature wavelength positions extracted from the outcrop and drill core spectra were further assessed by examining their correlation with distance to the nearest massive sulfide mineralization. Bivariate plots, shown in Figures 12A-B, show that rocks within the proximal areas display considerable variation in the Al-OH and Fe-OH wavelength positions. In

general, Figure 12A shows a lack of systematic spatial trends in the Al-OH absorption feature wavelength positions with distance to the mineralization. In contrast to this, the Fe-OH absorption feature wavelength positions display a shift toward longer wavelengths in the intermediate areas, and a shift toward shorter wavelengths in the areas distal (5700-6800 m) from mineralization (Fig. 12 B).

5. Discussion

5.1 Spectral characteristics of white micas and biotite/chlorite

The wavelength positions of the Al-OH absorption features of the outcrop and drill core spectra span a continuous wavelength range from 2194 nm to 2216 nm. According to Herrmann et al. (2001), this range corresponds to white micas that span in composition from sodic (paragonitic, or: high octahedral Al) to potassic to phengitic (low octahedral Al) muscovite. Similarly, the Fe-OH absorption feature wavelength positions, attributed to biotite and chlorite, display a wide and continuous range from 2244 nm to 2260 nm. Jones et al. (2005) suggested that this wavelength range represents compositional variability from Mg-rich to Fe-rich chlorite in the short and long end of the wavelength range, respectively.

The chemical compositional variations of these phyllosilicate minerals in the host rocks in and around the Izok Lake deposit are expressed as considerable vertical and horizontal spectral diversity in the immediate vicinity of the massive sulfide lenses (Fig. 12A,B), likely induced by intense hydrothermal alteration at varying temperatures and chemical gradients. Similar hydrothermal alteration-induced spectral variation has been documented in the Rosebery, Western Tharsis and Highway-Reward (Australia; Herrmann et al., 2001), Myra Falls (Canada; Jones et al., 2005) and Panorama

(Australia, Van Ruitenbeek et al., 2012) VMS deposits.

The vertical alteration intensity variation, as measured by the CCPI, indicates relatively weak alteration near the surface and intense alteration in the subsurface in the immediate vicinity of massive sulfide mineralization at approximately 100 m depth. This relationship can be explained by the occurrence of progressively higher temperatures at depth of circulating hydrothermal fluids at the time of hydrothermal alteration.

In the drill core spectra, the white micas in the immediate vicinity of the areas proximal to mineralization have short Al-OH wavelength positions, whereas those in the intermediate areas have relatively long Al-OH wavelength positions. The intermediate zone, interpreted to be a marginal discharge area by Laakso et al. (2015), is associated with intense hydrothermal alteration (Fig. 11C) that may have occurred at high temperatures and high water/rock ratios synchronous with deposit formation. In the distal areas, the AI values decrease and the Al-OH wavelength positions shift to slightly shorter wavelengths, consistent with a more potassic white mica composition.

In contrast to the spatial patterns of the Al-OH absorption features of the white micas, the Fe-OH wavelength positions of biotite/chlorite serve as a better-defined vector to mineralization in the Izok Lake deposit area. The spatial patterns of the Fe-OH absorption feature wavelength positions can be summarized as follows: the most proximal alteration is characterized by relatively short Fe-OH absorption feature wavelength positions that show considerable small-scale diversity, whereas the intermediate areas show a shift toward longer Fe-OH absorption feature wavelength positions. In the areas distal from mineralization there is a shift toward shorter Fe-OH absorption feature wavelengths. These findings can be interpreted as follows: intense alteration in the proximal areas is characterized by Mg-rich biotite/chlorite, whereas the

areas between the proximal and distal areas have intermediate to Fe-rich biotite and chlorite, and the distal areas also contain Mg-rich biotite/chlorite.

As discussed above, both the Al-OH and Fe-OH absorption feature wavelength positions show a shift toward longer wavelengths in the intermediate areas. In these areas, these trends are associated with a shift toward higher AI values of up to 98% that indicate almost wholesale replacement of feldspars and glass by sericite and chlorite (Large et al., 2001). In contrast, the northwestern parts of the study area display relatively weak AI values of 50-80%, and long Al-OH and Fe-OH absorption feature wavelength positions (up to 2209 nm and 2256 nm, respectively; Fig. 11A-C).

The highly variable physicochemical parameters of the hydrothermal systems from which VMS deposit form result in myriad and variable documented alteration styles and extents. For example, although Fe-rich chlorite has been documented in close proximity to some massive sulfide lenses (e.g., Plimer and de Carvalho, 1982; MacLean and Hoy, 1991; Leistel et al., 1998), other studies have documented Mg-chlorite in these areas (e.g. Date et al., 1983; Urabe et al., 1983; McLeod et al., 1987; Schmidt, 1988; Sánchez-España et al., 2000; Paulick et al., 2001; Hannington et al., 2003; Biel et al., 2010). Regardless of the chemical composition of chlorite, altered rocks in the proximal fluid upflow areas can have white micas that are either predominantly Al-rich (e.g., Urabe et al., 1983; Jones et al., 2005; Herrmann et al., 2009) or Al-poor (e.g. Biel et al., 2010). Similar trends to those present in the compositional variety of the white micas and biotite/chlorite group minerals of the Izok Lake deposit have been reported from other VMS deposits such as the South Bay deposit in Ontario, Canada (Urabe et al., 1983) and the Ambler mineral district in Alaska (Schmidt, 1988).

5.2 Correlations between spectral absorption features and bulk rock compositions

One of the limitations of the CCPI is that it is strongly affected by primary

compositional variations in the volcanic rocks (Large et al., 2001). This phenomenon is also evident in the alteration box plot (Fig. 9), in which the intermediate and mafic volcanic rocks of the study area (andesite and basalt) predominantly group in the high CCPI and low AI corner of the plot. As such rock types contain more ferromagnesian minerals than the felsic volcanic rocks (e.g., rhyolite), the high CCPI values in these rocks are controlled predominantly by their primary mineralogy and not the intensity of alteration. However, lithologic variation plays a minimal role in our study because care was taken to analyze only the lithogeochemical and spectral properties of the rhyolitic rocks. This is also evidenced by the Winchester-Floyd diagram that indicates the predominantly rhyolitic character of the outcrop lithogeochemical samples (Fig. 8).

Despite its limitations, the CCPI is designed to measure chloritic alteration (Large et al., 2001), and hence is well suited to the study of hydrothermal alteration in VMS deposits. In our study, the CCPI was chosen over the AI to estimate the alteration intensity variation of the drill cores because there is no discernable correlation between AI and VEAI, whereas there is a good correlation between the CCPI and VEAI. The presence of chloritic alteration in the vicinity of the Izok Lake massive sulfide lenses (Morrison, 2004) best explains the correlation between CCPI and VEAI.

The weak negative correlation between the Al-OH absorption feature wavelengths of the drill core spectra and the CCPI indicates that increasing alteration intensity is associated with increasing Al content of the white micas. Yang et al. (2011) have documented a similar relationship between the Al-OH absorption feature wavelength positions of andesitic host rocks and the AI in Hellyer VMS deposit, Tasmania. Herrmann et al. (2001) reported an inverse correlation between the Al-OH wavelength positions and the AI values of the Western Tharsis (Tasmania) and Highway-Reward (Queensland, Australia) deposits. The investigation by Herrmann et

al. (2001) in the Rosebery deposit (Tasmania) found no association between the lithogeochemical and spectral datasets. Despite the correlation between the Al-OH absorption feature wavelength positions of the drill core data and the nearest lithogeochemical data at Izok Lake, the lack of a quantifiable relationship between the Al-OH absorption features of the outcrop spectral dataset and the AI suggests that the chemical composition of the white micas is an imperfect mineral exploration vectoring tool in the study area.

Correlations between the Fe-OH wavelength positions of the spectral datasets (outcrop and drill core) and the AI and CCPI alteration indices show statistically significant positive correlations, suggesting that high alteration intensities are in general associated with a shift toward a more Fe-rich biotite/chlorite in the study area. The observed iron enrichment of these phyllosilicate minerals can result from several factors, such as their formation in a high-temperature discharge zone that was characterized by Fe-rich hydrothermal fluids at the time of hydrothermal alteration.

Despite the presence of some Fe-rich biotite and chlorite, the phyllosilicate minerals associated with the highest AI and CCPI values (80-100%) have average absorption feature wavelength positions of 2253 nm and 2254 nm for the drill core and outcrop spectral datasets, respectively, indicative of Mg-rich compositions (Yang and Huntington, 1996; Figs. 6B and 10B). Hence, the observed shift toward a more Fe-rich composition is relative and does not imply that the most intense alteration is associated with iron-rich chlorite and biotite. It is noteworthy that the areas proximal and distal to the Izok Lake mineralization are characterized by high and low hydrothermal alteration intensity values, respectively (Fig. 11C), but both areas have Mg-rich biotite/chlorite that are spectrally similar (Fig. 12B). Hence, without the lithogeochemical data and field observations, the distal areas might have been (mis)interpreted as being favourable to

hosting mineralization. Our study therefore highlights the importance of using all available geological, geochemical and mineralogical information in the application of hydrothermal alteration vectoring toward VMS mineralization.

There are a number of external factors that influence our results. First, a relatively small number of observations and data are available, and hence caution should be exercised when interpreting the correlations between outcrop spectral and lithogeochemical features both in the Izok Lake area and elsewhere. If the chemical compositions of the white micas and biotite/chlorite do not vary exclusively as a function of the alteration processes, the correlations between the spectral and lithogeochemical data can reflect multiple factors that include (but are not limited to) hydrothermal alteration. One factor potentially affecting the mineralogy of VMS deposits is metamorphism that can recrystallize and re-equilibrate minerals at metamorphic conditions that exceed greenschist facies (Dusel-Bacon, 2012). Evaluation of the metamorphic overprint of the Izok Lake study area is out of scope of this investigation, and can be found elsewhere. For instance, the investigation by Nowak (2012) suggests that amphibolite-facies metamorphism resulted in only minor changes in the chemical compositions of the rocks in the study area.

Another factor that may potentially influence the relationship between the spectroscopic and lithogeochemical data is the sampling interval. The average distance between the outcrop spectral measurement and the nearest lithogeochemical data is 50.5 m, and this relatively large distance may have weakened the relationship between these two datasets. In contrast, the average distance between the drill core spectral measurements and the nearest lithogeochemical data is only 3 m, indicating that local variations in alteration type and intensity play only a minor role in the correlations between the spectral and lithogeochemical data extracted from the drill cores.

5.3 Implications of the spectral features for deposit genesis

Iron enrichment is common in the highly altered discharge areas of VMS deposits that typically contain Fe-rich chlorite (MacLean and Hoy, 1991; Barrett and MacLean, 1994). In the Izok Lake deposit, however, our infrared spectroscopic data indicate that the proximal areas contain more Mg-rich chlorite and biotite than the intermediate areas farther away from the mineralization. This conclusion is supported by the findings of Money and Heslop (1976), who reported Mg-enrichment in rocks proximal to the deposit. Several studies (Schmidt, 1988; Schade et al., 1989; Paulick et al., 2001; Hannington et al., 2003) have similarly noted Mg-enrichment in the vicinity of the feeder (fluid upflow) zones of VMS deposits, and attributed these patterns to the influx of seawater.

Paleo-hydrothermal upflow and discharge zones generally display the highest alteration intensities in VMS deposits (Barrett and MacLean, 1994), and therefore an area of strong alteration located west of the known massive sulfide lenses (Fig. 11C) merits further exploration, as it may be associated with yet unrecognized mineralization.

6. Conclusions

Outcrop and drill core spectroscopy of the host rocks to the Izok Lake VMS deposit display a wide spectral range of the Al-OH and Fe-OH absorption feature wavelength positions that indicate considerable compositional variation within the contained phyllosilicate minerals. This variation is attributable to variable parameters during the hydrothermal alteration process, possibly including the physico-chemical composition of the hydrothermal fluids, water/rock-ratios and temperature that have influenced the mineralogical and chemical composition of the alteration minerals. These

processes have resulted in the formation of Al-rich white micas and Mg-rich biotite/chlorite in the intensely altered rocks of the proximal areas. The Mg-rich compositions of chlorite and biotite may be due to influx of seawater that resulted in Mg-metasomatism. Further away from the proximal alteration is a zone of Al-poor white micas and intermediate to Fe-rich biotite and chlorite that transitions to a distal zone of predominantly potassic muscovite and Mg-rich biotite and chlorite.

The weak positive correlation between the Fe-OH absorption feature wavelength positions and the alteration intensity (using AI and CCPI as proxies) is evident in both the outcrop and drill core spectral datasets. There is also a statistically significant correlation between the Al-OH absorption feature wavelength positions of the drill core spectrometry and alteration intensity, but this is only evident in the drill core spectra, and not the outcrop spectra. Hence, in the study area, the spectral properties of chlorite and biotite follow the alteration intensity variation more closely than those of the white micas. Although the correlation coefficients for the relationships between the Al-OH/Fe-OH absorption feature wavelength positions and the alteration indices are weak, the Al-OH and Fe-OH wavelength positions of the white micas and biotite/chlorite, respectively, do provide a useful measure of the alteration intensity of the rocks that host the Izok Lake VMS deposit. However, the weak correlations between the Al-OH and Fe-OH absorption feature wavelength positions and the AI and CCPI alteration indices suggest that the spectral shifts detected in these phyllosilicate minerals are better suited for inferring large-scale rather than small-scale alteration patterns. Moreover, because VMS deposits can have differing alteration fingerprints due to the complexity of factors that induce hydrothermal alteration, caution should be exercised, and a baseline study is recommended before applying the conclusions for Izok Lake to other VMS deposits elsewhere.

Acknowledgements

This work was funded through the Research Affiliate Program of the Earth Sciences Sector of Natural Resources Canada (2011-2013), the Targeted Geoscience Initiative 4 (TGI-4) Program of the Earth Sciences Sector, Natural Resources of Canada (2013-2014), and a discovery grant to Benoit Rivard from the National Science and Engineering Research Council of Canada. We thank MMG Ltd., particularly Trish Toole, Ian Neill, and Dave Kelley, for logistical and field support in 2010 and 2013, and for geological discussions and access to their lithogeochemical and drill core data. We thank Jeanne B. Percival (Geological Survey of Canada), Bernard Hubbard and Dr. Lyle Mars (both United States Geological Survey), and an anonymous reviewer who helped us greatly improve the manuscript. This is Geological Survey of Canada contribution number 20150300.

References

Barrett, T.J., and MacLean, W.H., 1994, Chemostratigraphy and hydrothermal alteration in exploration for VHMS deposits in greenstones and younger volcanic rocks, in Lentz, D.R., ed., Alteration and alteration processes associated with ore-forming Systems: Geological Association of Canada, Short Course Notes 11, p. 433–467.

Bassett, W.A., 1960, Role of hydroxyl orientation in mica alteration: Bulleting of the Geological Society of America, v. 71, p. 449–456.

Biel, C., Subías, I., Fanlo, I., Mateo, E., and Acevedo, R.D., 2010, The Arroyo Rojo volcanic-hosted massive sulphide deposit (Tierra del Fuego, southernmost Argentina): geology, mineralogy, petrography and mineral chemistry: Revista Mexicana de Ciencias Geológicas, v. 27, p. 84–96.

Bostock, H.H., 1980, Geology of the Itchen Lake area, district of Mackenzie. Geological Survey of Canada Memoir 391: Canadian Government Publishing Centre, Ottawa, Canada, 101 p.

Bruegge, C.J., Stiegman, A.E., Rainen, R.A., and Springsteen, A.W., 1993, Use of Spectralon as a diffuse reflectance standard for in-flight calibration of earth-orbiting sensors: Optical Engineering, v. 32, p. 805-814.

Cathelineau, M., 1988, Cation site occupancy in chlorites and illites as a function of temperature: Clay Minerals, v. 23, p. 471–485.

Clark, R.N., 1999, Chapter 1: Spectroscopy of rocks and minerals, and principles of spectroscopy, in Rencz, A.N., ed., Manual of remote sensing, Volume 3. Remote Sensing for the Earth Sciences: John Wiley and Sons, New York, p. 3–58.

Clark, R.N., Swayze, G.A., Livo, K.E., Kokaly, R.F., King, T.V.V., Dalton, J.B., Vance, J.S., Rockwell, B.W., Hoefen, T., and McDougal, R.R., 2002, Surface reflectance calibration of terrestrial imaging spectroscopy data: A tutorial using AVIRIS, in:

Proceedings of the 10th Airborne Earth Science Workshop, JPL (Jet Propulsion Laboratory) Publication 02-1, Pasadena, USA, 2002.

Date, J., Watanabe, Y., and Saeki, Y., 1983, Zonal alteration around the Fukazawa Kuroko deposits, Akita prefecture, northern Japan: Economic Geology Monography, v. 5, p. 365–386.

Duke, E.F., 1994, Near infrared spectra of muscovite, Tschermak substitution, and metamorphic reaction progress: Implications for remote sensing: Geology, v. 22, p. 621–624.

Dusel-Bacon, C., 2012, Petrology of metamorphic rocks associated with volcanogenic massive sulfide deposits, in Shanks, W.C.P. III, and Thurston, R., eds., Volcanogenic massive sulfide occurrence model: U.S. Geological Survey, Scientific Investigations Report 2010-5070-C, Chapter 17, 10 p.

Franklin, J., 1997, Lithogeochemical and mineralogical methods for base metal and gold exploration, in Gubins, A.G., ed., Proceedings of Exploration 97: Fourth Decennial International Conference on Mineral Exploration, Toronto, Canada, 1997, p. 191–208.

Franklin, J.M., Kasarda, J., and Poulsen, K.H., 1975, Petrology and chemistry of the alteration zone of the Mattabi massive sulfide deposit: Economic Geology, v. 70, p. 63–79.

Galley, A.G., 1993, Characteristics of semi-conformable alteration zones associated with volcanogenic massive sulphide districts: Journal of Geochemical Exploration, v. 48, p. 175–200.

Galley, A.G., Hannington, M.D., and Jonasson, I.R., 2007, Volcanogenic massive sulphide deposits, in Goodfellow, W.D., ed., Mineral deposits of Canada: A synthesis of major deposit-types, district metallogeny, the evolution of geological provinces, and exploration methods. Geological Association of Canada, Mineral

Deposits Division, Special Publication No. 5, Ottawa, Canada, p. 141-161.

Gemmell, J.B., and Large, R.R., 1992, Stringer system and alteration zones underlying the Hellyer volcanic-hosted massive sulfide deposit, Tasmania, Australia: Economic Geology, v. 87, p. 620–649.

Goodfellow, W.D., and Peter, J.M., 1994, Geochemistry of hydrothermally altered sediment, Middle Valley, northern Juan de Fuca Ridge, in: Mottl, M.J., Davis, E.E., Fisher, A.T. and Slack, J.F., eds., Proceedings of the Ocean Drilling Program, Scientific Results, v. 139. Texas A&M University, College Station, Texas, p. 207–289.

Hannington, M.D., Kjarsgaard, I.M., Galley, A.G., and Taylor, B., 2003, Mineral-chemical studies of metamorphosed hydrothermal alteration in the Kristineberg volcanogenic massive sulfide district, Sweden: Mineralium Deposita, v. 38, p. 423–442.

Herrmann, W., Blake, M., Doyle, M., Huston, D., Kamprad, J., Merry, N., and Pontual, S., 2001, Short wavelength infrared (SWIR) spectral analysis of hydrothermal alteration zones associated with base metal sulfide deposits at Rosebery and Western Tharsis, Tasmania, and Highway-Reward, Queensland: Economic Geology, v. 96, p. 939–955.

Herrmann, W., Green, G.R., Barton, M.D., and Davidson, G.J., 2009, Lithogeochemical and stable isotopic insights into submarine genesis of pyrophyllite-altered facies at the Boco Prospect, Western Tasmania: Economic Geology, v. 104, p. 775–792.

Hunt, G.R., and Salisbury, J.W., 1970, Visible and near-infrared spectra of minerals and rocks: I. Silicate minerals: Modern Geology, v. 1, p. 283–300.

Ishikawa, Y., Sawaguchi, T., S.-i., Iwaya, and Horiuchi, M., 1976, Delineation of prospecting targets for Kuroko deposits based on modes of volcanism of underlying dacite and alteration haloes: Mining Geology, v. 26, p. 105–117.

Jones, S., Herrmann, W., and Gemmell, J.B., 2005, Short wavelength infrared spectral characteristics of the HW horizon: Implications for exploration in the Myra Falls volcanic-hosted massive sulfide camp, Vancouver Island, British Columbia, Canada: Economic Geology, v. 100, p. 273–294.

Kranidiotis, P., and MacLean, W.H., 1987, Systematics of chlorite alteration at the Phelps Dodge massive sulfide deposit, Matagami, Quebec: Economic Geology, v. 82, p. 1898–1911.

Laakso, K., Rivard, B., Peter, J.M., White, H.P., Maloley, M., Harris, J., and Rogge, D., 2015, Application of airborne, laboratory and field hyperspectral methods to mineral exploration in the Canadian Arctic: Recognition and characterization of volcanogenic massive sulfide-associated hydrothermal alteration in the Izok Lake deposit area, Nunavut, Canada: Economic Geology, v. 110, p. 925-941.

Large, R.R., 1977, Chemical evolution and zonation of massive sulfide deposits in volcanic terrains: Economic Geology, v. 72, p. 549–572.

Large, R.R., Gemmell, J.B., Paulick, H., and Huston, D.L., 2001, The alteration box plot: A simple approach to understanding the relationship between alteration mineralogy and lithogeochemistry associated with volcanic-hosted massive sulfide deposits: Economic Geology, v. 96, p. 957–971.

Leistel, J.M., Marcoux, E., Thiéblemont, D., Quesada, C., Sánchez, A., Almodóvar, G.R., Pascual, E., and Sáez, R., 1998, The volcanic-hosted massive sulphide deposits of the Iberian Pyrite Belt: Mineralium Deposita, v. 33, p. 2–30.

MacLean, W.H., and Hoy, L.D., 1991, Geochemistry of hydrothermally altered rocks at the Horne Mine, Noranda, Quebec: Economic Geology, v. 86, p. 506–528.

McLeod, R.L., Gabell, A.R., Green, A.A., and Gardavsky, V., 1987, Chlorite infrared spectral data as proximity indicators of volcanogenic massive sulphide mineralisation. Pacific Rim Congress (The Geology, Structure, Mineralisation and

Economy of the Pacific Rim): Australian Institute of Mining and Metallurgy, Gold Coast, Australia, 1987, p. 321–324.

Miyashiro, A., and Shido, F., 1985, Tschermak substitution in low- and middle-grade pelitic schists: Journal of Petrology, v. 26, p. 449–487.

MMG Ltd., 2011, Izok Lake. A summary of exploration activity on the Izok Lake project 2007-2011, 2011 Annual Report Nunavut Impact Review Board. (http://ftp.nirb.ca/01-screenings/completed%20screenings/2006/06EN066MMG (Wolfden)-Izok%20and%20Hood%20Project/05ANNUAL%20REPORT/120201-06EN066-MMG%202011%20Annual%20Report-IA1E.pdf).

Money, P.L., and Heslop, J.B., 1976, Geology of the Izok Lake massive sulphide deposit: Canadian Mining Journal, v. 97, p. 24–27.

Morrison, I.R., 2004, Geology of the Izok massive sulfide deposit, Nunavut Territory, Canada: Exploration and Mining Geology, v. 13, p. 25–36.

Mortensen, J.K., Thorpe, R.I., Padgham, W.A., King, J.E., and Davis, W.J., 1988, U-Pb zircon ages for felsic volcanism in Slave Province, N.W.T., in Radiogenic Age and Isotopic Studies: Report 2: Geological Survey of Canada 88-2, p. 85–95.

Nowak, R., 2012, The nature and significance of high-grade metamorphism and intense deformation on the Izok VHMS alteration halo and deposit: Unpublished M.Sc. thesis, Colorado School of Mines, 194 p.

Ohmoto, H., 1996, Formation of volcanogenic massive sulfide deposits: The Kuroko perspective: Ore Geology Reviews, v. 10, p. 135–177.

Oliver, M.A., and Webster, R., 1990, Kriging: a method of interpolation for geographical information systems: International Journal of Geographical Information Systems, v. 4, p. 313–332.

Paulick, H., Herrmann, W., and Gemmell, J.B., 2001, Alteration of felsic volcanics hosting the Thalanga massive sulfide deposit (Northern Queensland, Australia) and

geochemical proximity indicators to ore: Economic Geology, v. 96, p. 1175–1200.

Pirajno, F., 2009, Hydrothermal processes and wall rock alteration, in Hydrothermal Processes and Mineral Systems. Springer Netherlands, p. 73-164.

Plimer, I.R., and de Carvalho, D., 1982, The geochemistry of hydrothermal alteration at the Salgadinho Copper Deposit, Portugal: Mineralium Deposita, v. 17, p. 193–211.

Post, J.L., and Noble, P.N., 1993, The near-infrared combination band frequencies of dioctahedral smectites, micas, and illites: Clays and Clay Minerals, v. 41, p. 639–644.

Sánchez-España, J., Velasco, F., and Yusta, I., 2000, Hydrothermal alteration of felsic volcanic rocks associated with massive sulphide deposition in the northern Iberian Pyrite Belt (SW Spain): Applied Geochemistry, v. 15, p. 1265–1290.

Schade, J., Cornell, D.H., and Theart, H.F.J., 1989, Rare earth element and isotopic evidence for the genesis of the Prieska massive sulfide deposit, South Africa: Economic Geology, v. 84, p. 49–63.

Schmidt, J.M. 1988, Mineral and whole-rock compositions of seawater-dominated hydrothermal alteration at the Arctic volcanogenic massive sulfide prospect, Alaska: Economic Geology, v. 83, p. 822–842.

Seyfried, W.E., Jr., Berndt, M.E., and Seewald, J.S., 1988, Hydrothermal alteration processes at mid-ocean ridges: Constraints from diabase alteration experiments, hot spring fluids and composition of the oceanic crust: Canadian Mineralogy, v. 26, p. 787–804.

Shapiro, S.S. and Wilk, M.B., 1965, An analysis of variance test for normality (complete samples): Biometrika, v. 52, p. 591-611.

Stephens, M.B., Swinden, H.S., and Slack, J.F., 1984, Correlation of massive sulfide deposits in the Appalachian-Caledonian Orogen on the basis of Paleotectonic setting: Economic Geology, v. 79, p. 1442–1478.

Urabe, T., Scott, S.D., and Hattori, K., 1983, A comparison of footwall-rock alteration and geothermal systems beneath some Japanese and Canadian volcanogenic massive sulfide deposits: Economic Geology. Monograph., v. 5, p. 345–364.

Van Ruitenbeek, F.J.A., Cudahy, T.J., Van der Meer, F.D. and Hale, M., 2012, Characterization of the hydrothermal systems associated with Archean VMS-mineralization at Panorama, Western Australia, using hyperspectral, geochemical and geothermometric data: Ore Geology Reviews, v. 45, p. 33-46.

Velde, B., 1965, Phengite micas: Synthesis, stability, and natural occurrence: American Journal of Science, v. 263, p. 886–913.

Winchester, J.A. and Floyd, P.A., 1977, Geochemical discrimination of different magma series and their differentiation products using immobile elements: Chemical Geology, v. 20, p. 325-343.

Yang, K., and Huntington, J.F., 1996, Spectral signatures of hydrothermal alteration in the metasediments at Dead Bullock Soak, Tanami Desert, Northern Territory. CSIRO Division of Exploration and Mining, Australia, 29 p.

Yang, K., Huntington, J.F., Gemmell, J.B., and Scott, K.M., 2011, Variations in composition and abundance of white mica in the hydrothermal alteration system at Hellyer, Tasmania, as revealed by infrared reflectance spectroscopy: Journal of Geochemical Exploration, v. 108, p. 143–156.

FIGURE LEGENDS

Figure 1. Location map and geological map of the Izok Lake study area showing the locations of the outcrop spectrosopic sites, samples, drill cores and lithogeochemical samples. meas.=measurement.

Figure 2. Location of the drill cores and sulfide lenses. The geology and projected location of massive sulfide zones are from MMG Ltd. unpublished GIS data.

Figure 3. A) Reflectance spectra from drill cores HEN187 ("HEN187-0018", spectrum 1) and HEN-186 ("HEN186-0014", spectrum 2); B) Selected range plot of hull quotient-corrected spectra 1 (absorption feature wavelength position: 2208 nm) and 2 (absorption feature wavelength position: 2195 nm) shown in A; C) Reflectance spectra from drill cores HEN252 ("HEN252-0012", spectrum 1) and HEN-188 ("HEN188-0016", spectrum 2); D) Selected range plot of hull quotient-corrected spectra 1 (absorption feature wavelength position: 2259 nm) and 2 (absorption feature wavelength position: 2246 nm) shown in C.

Figure 4. Frequency distribution histograms of absorption band position for: A) drill core Al-OH absorption; B) drill core Fe-OH absorption; C) outcrop spectra Al-OH absorption; D) outcrop spectra Fe-OH absorption.

Figure 5. Bivariate plot of the visually estimated alteration intensity (VEAI) of the drill cores versus A) the calculated chlorite-carbonate-pyrite index (CCPI) (expressed as %); and B) the calculated Ishikawa index (AI) (expressed as %).

Figure 6. Bivariate plot of the chlorite-carbonate-pyrite index (CCPI, expressed as %) calculated from the lithogeochemical data for the drill core samples versus A) the Al-OH wavelength positions (in nm) and; B) the Fe-OH wavelength positions (in nm).

Figure 7. A vertical cross section of the lithogeochemical and spectral trends across seven drill cores (HEN-172, HEN-173, HEN-197, HEN-262, HEN-273, HEN-309

and HEN-340). A) map view of the locations of the drill cores; B) three-dimensional lithological map of the drill cores. Downhole variation of: C) Cu contents (ppm); D) chlorite-carbonate-pyrite index (CCPI, %) values; E) Al-OH absorption feature wavelength positions (nm); F) Fe-OH absorption feature wavelength positions (nm). pegmat.=pegmatite. The Cu contents of the drill cores are extracted across all lithologies and the CCPI, Al-OH and Fe-OH values are extracted from the rhyolitic rock sections of the drill cores. Due to the three dimensional nature of the profile, and the uncertainty on the spatial dimensions of the rock units, the interpolation results are displayed across different rock units for the full vertical section (0-200 m depth). These interpolations were created by estimating the value of each voxel node (three-dimensional cell) using the value of the nearest drill core observation (i.e. the "nearest neighbor"). All the sections face west.

Figure 8. Nb/Y (ppm) versus Zr/TiO_2 (ppm) discrimination plot of Winchester and Floyd (1977) for the lithogeochemical samples. Shown in the plot are the outcrop samples from the Izok Lake study area (*n*=555).

Figure 9. Alteration box plot of Large et al. (2001) showing lithogeochemical samples of the Izok Lake study area. bas.=basalt, dac.=dacite, pant.=pantellerite.

Figure 10 Bivariate plots of: A) the Al-OH absorption feature wavelengths of the outcrop spectra (*n*=357) versus the Ishikawa index (AI, expressed as %). The lithogeochemical samples represent rhyolite (*n*=347), rhyodacite-dacite (*n*=3) and comendite-pantellerite (*n*=7); B) the Fe-OH absorption feature wavelengths of the outcrop spectra (*n*=264) versus the AI (expressed as %). The lithogeochemical samples represent rhyolite (*n*=260) and comendite-pantellerite (*n*=4). All the spectral measurements (Figs. A and B) are acquired from the rhyolitic rocks.

Figure 11. Color gradient map of the absorption feature wavelength positions extracted

from the outcrop spectra for A) Al-OH and B) Fe-OH and subsetted to the spatial dimensions of the approximated extent of the rhyolitic rocks in the study area. Only areas proximal (327-2679 m) to the mineralization are shown in the interpolation due to the sparsity of data in the more distal areas. C) Color gradient map of the AI calculated from the lithogeochemical data for drill core and outcrop samples.

Figure 12. Bivariate plots of the absorption feature wavelength positions of the outcrop and drill core spectra versus distance from massive sulfide mineralization for A) Al-OH and B) Fe-OH.

TABLE LEGENDS

Table 1. Summary statistics of the Al-OH and Fe-OH absorption features of the outcrop and drill core spectra.

Figure 1

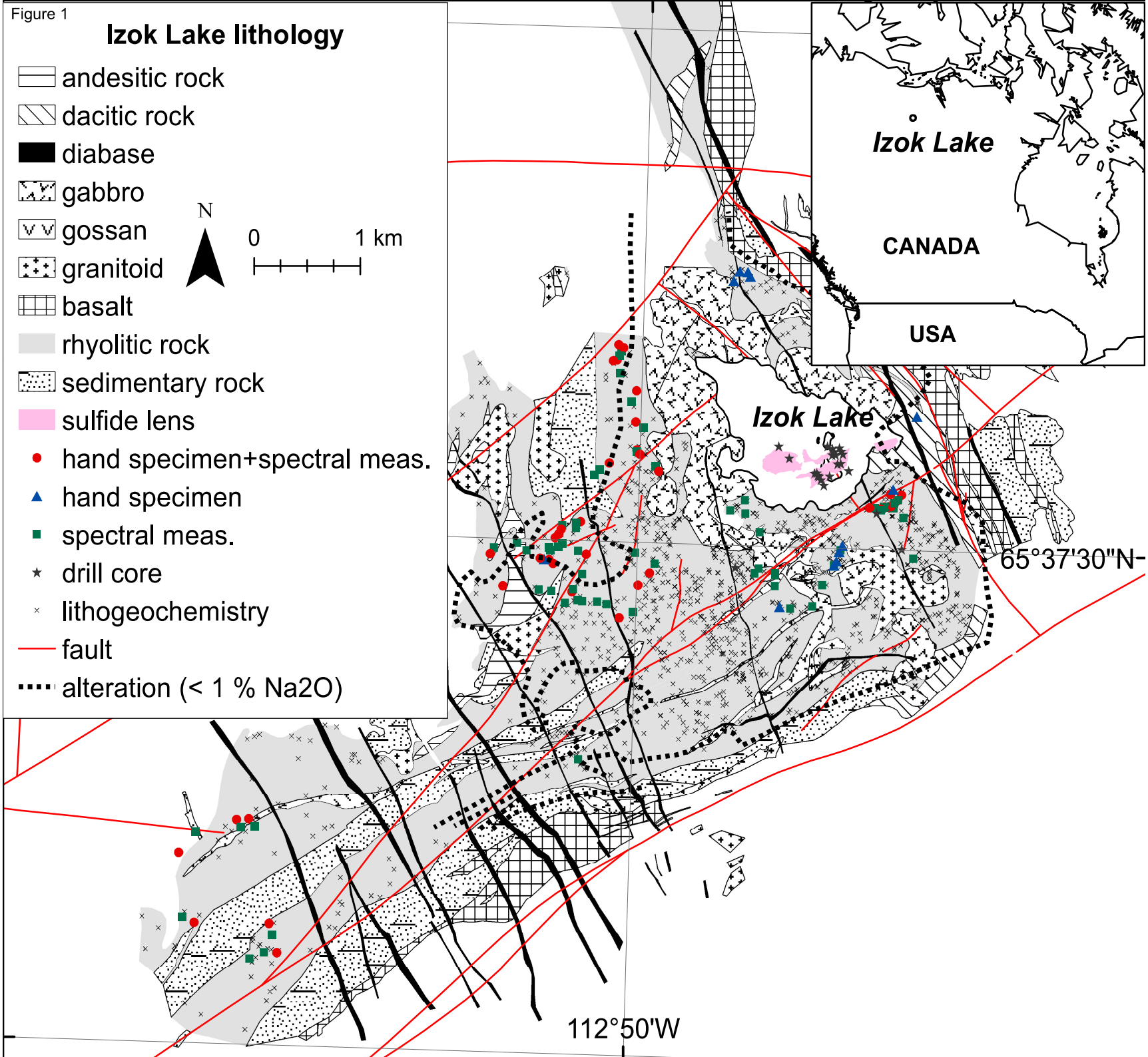
Izok Lake lithology
andesitic rock
dacitic rock
diabase
gabbro
gossan
granitoid
basalt
rhyolitic rock
sedimentary rock
sulfide lens
hand specimen+spectral meas.
hand specimen
spectral meas.
drill core
lithogeochemistry
fault
alteration (< 1 % Na2O)
N
0
1 km
Izok Lake
CANADA
USA
Izok Lake
65°37'30"N
112°50'W

Figure 2

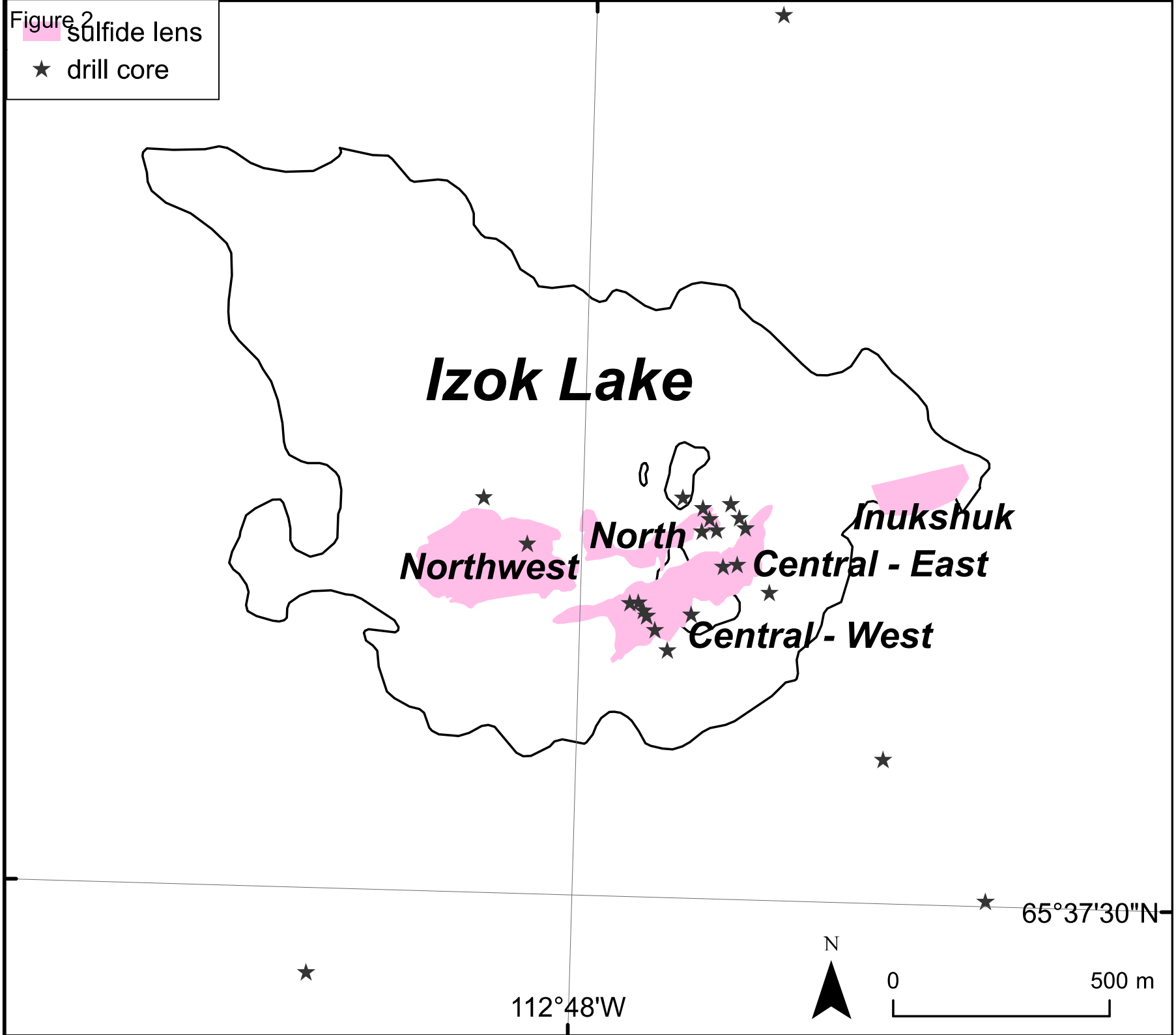
sulfide lens
drill core
Izok Lake
Northwest
North
Central - East
Central - West
Inukshuk
65°37'30"N
112°48'W
N
0
500 m

Figure 3

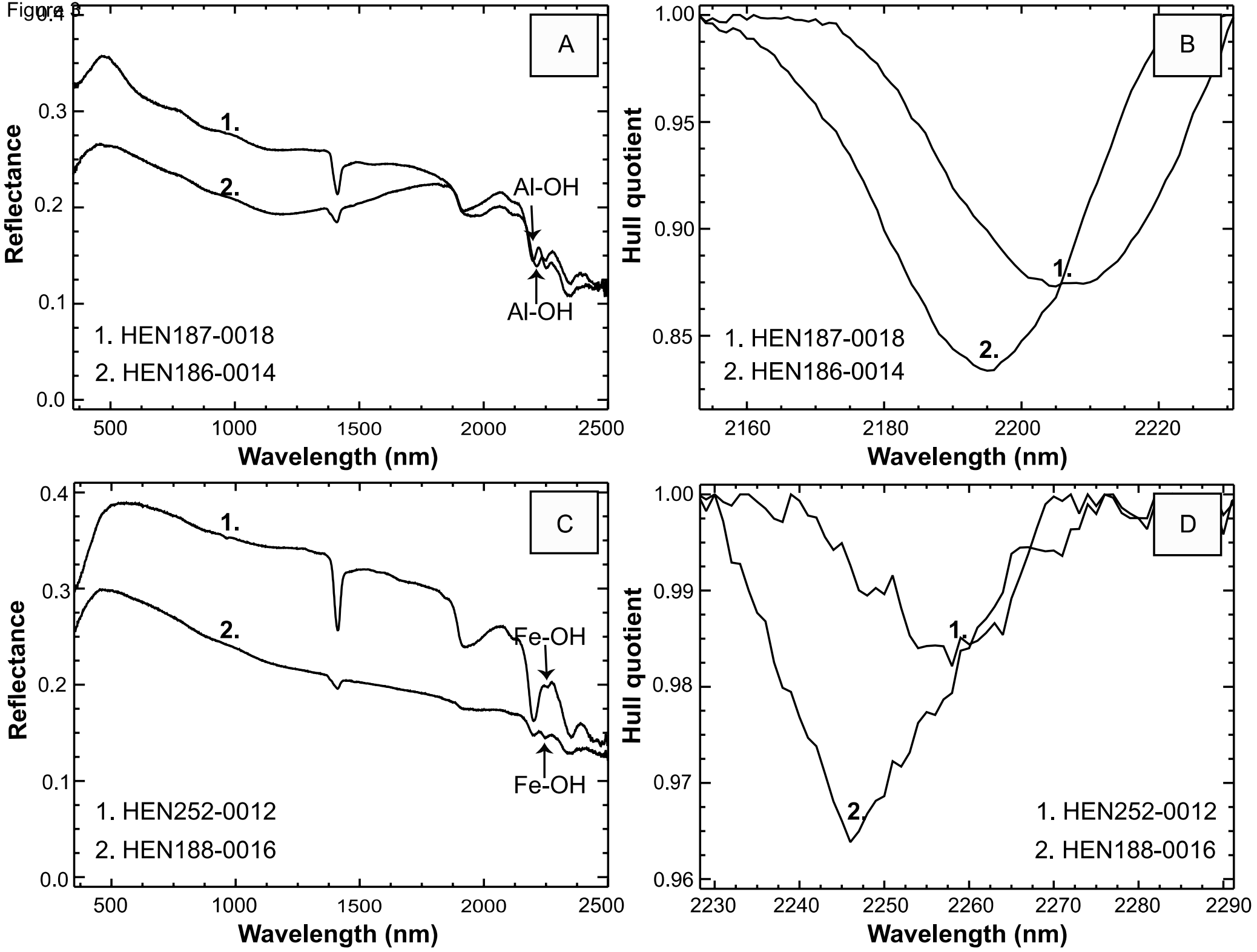
A
Reflectance
Wavelength (nm)
1.
2.
Al-OH
Al-OH
1. HEN187-0018
2. HEN186-0014
B
Hull quotient
Wavelength (nm)
1.
2.
1. HEN187-0018
2. HEN186-0014
C
Reflectance
Wavelength (nm)
1.
2.
Fe-OH
Fe-OH
1. HEN252-0012
2. HEN188-0016
D
Hull quotient
Wavelength (nm)
1.
2.
1. HEN252-0012
2. HEN188-0016

Figure 4

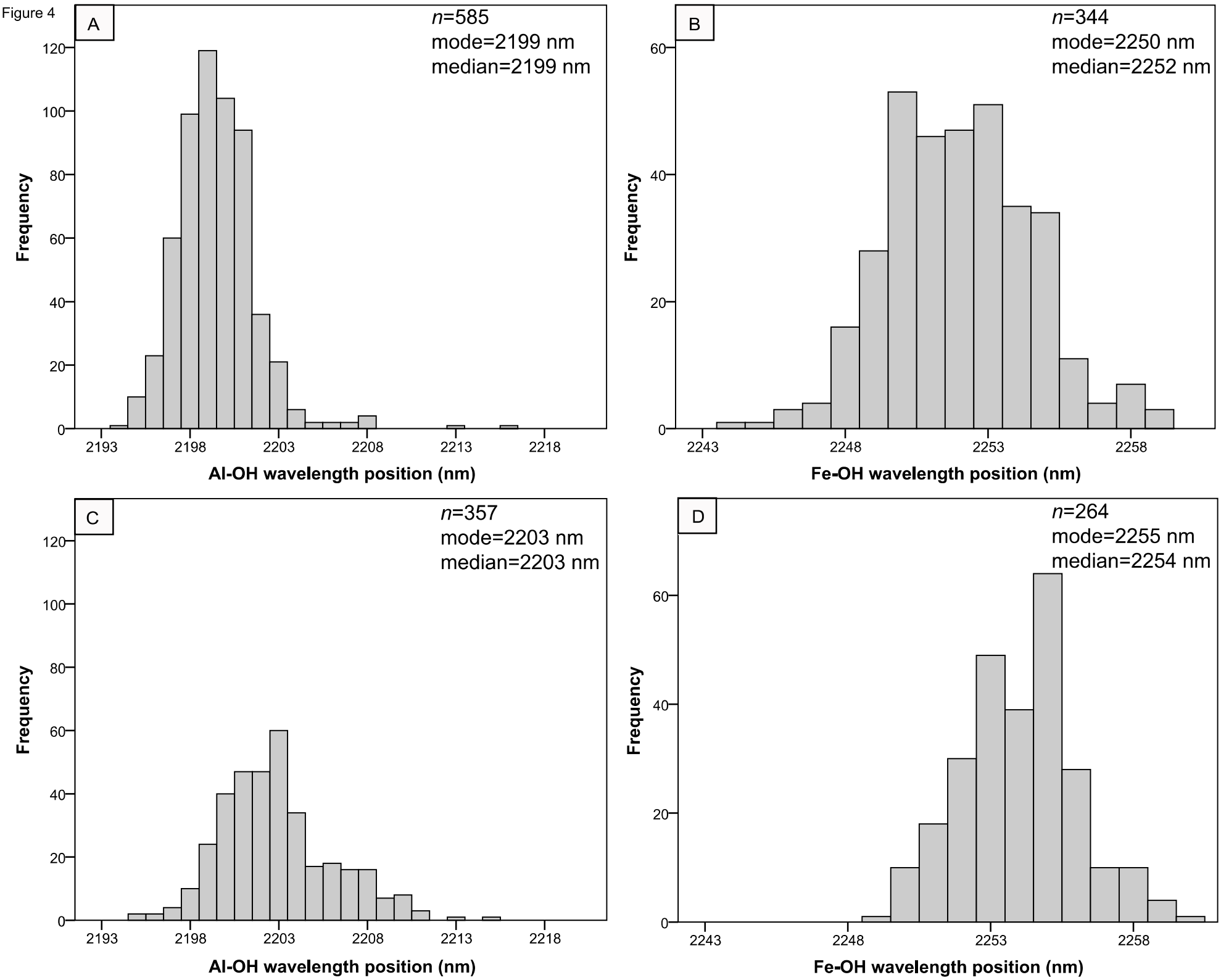
A
n=585
mode=2199 nm
median=2199 nm
Frequency
Al-OH wavelength position (nm)
B
n=344
mode=2250 nm
median=2252 nm
Frequency
Fe-OH wavelength position (nm)
C
n=357
mode=2203 nm
median=2203 nm
Frequency
Al-OH wavelength position (nm)
D
n=264
mode=2255 nm
median=2254 nm
Frequency
Fe-OH wavelength position (nm)

Figure 5

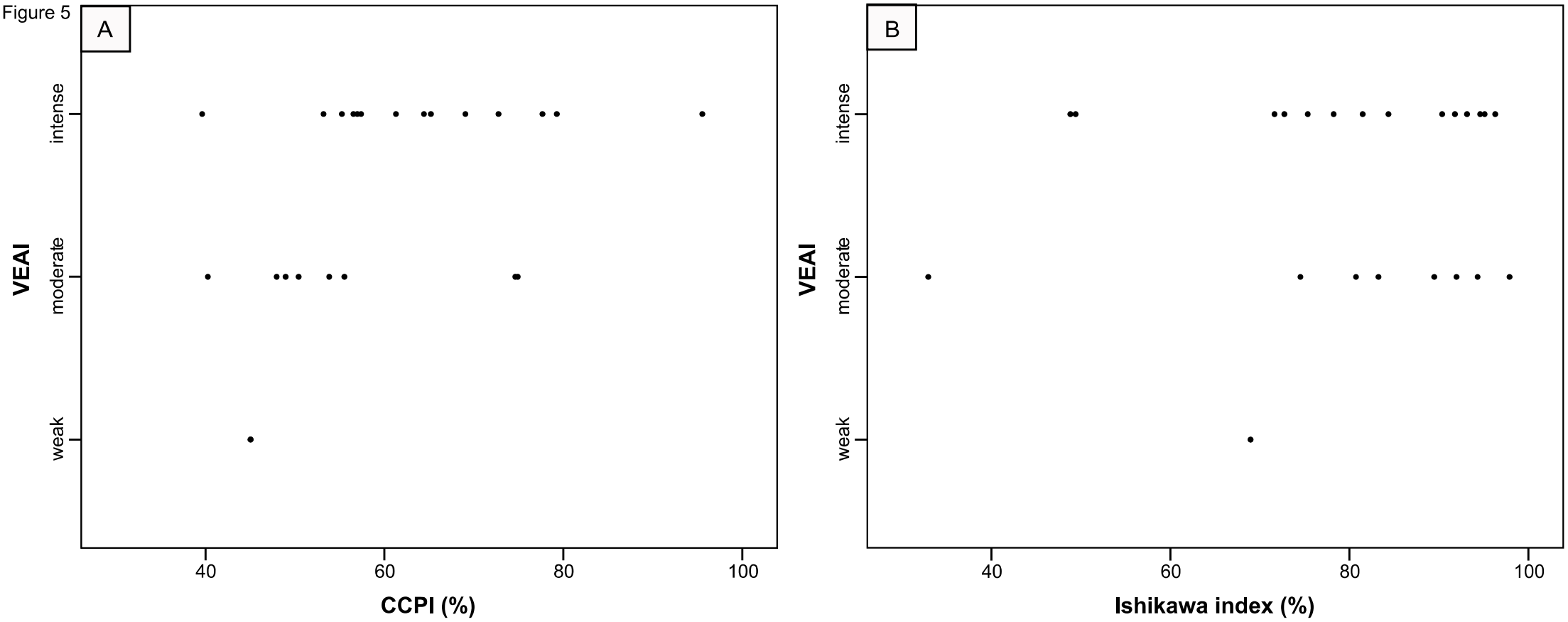
A
B
VEAI
intense
moderate
weak
40
60
80
100
CCPI (%)
Ishikawa index (%)

Figure 6

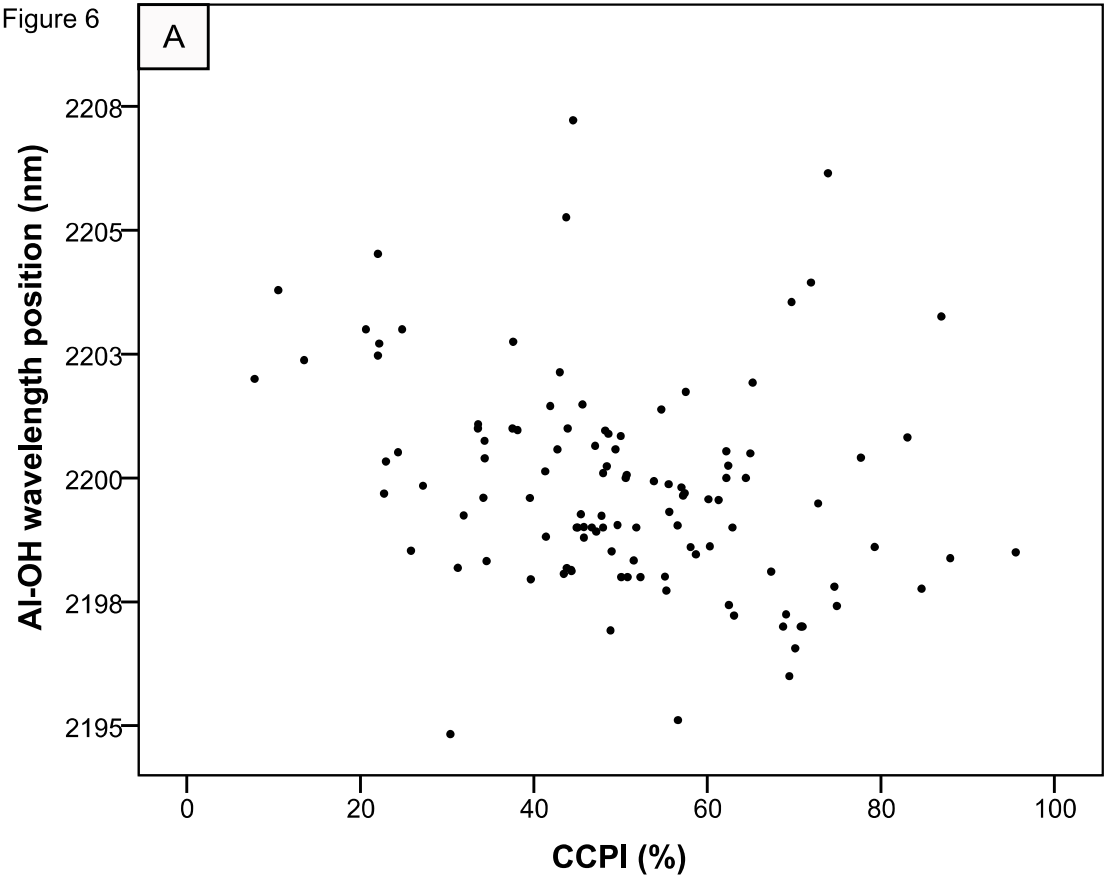
A
Al-OH wavelength position (nm)
2208
2205
2203
2200
2198
2195
0
20
40
60
80
100
CCPI (%)

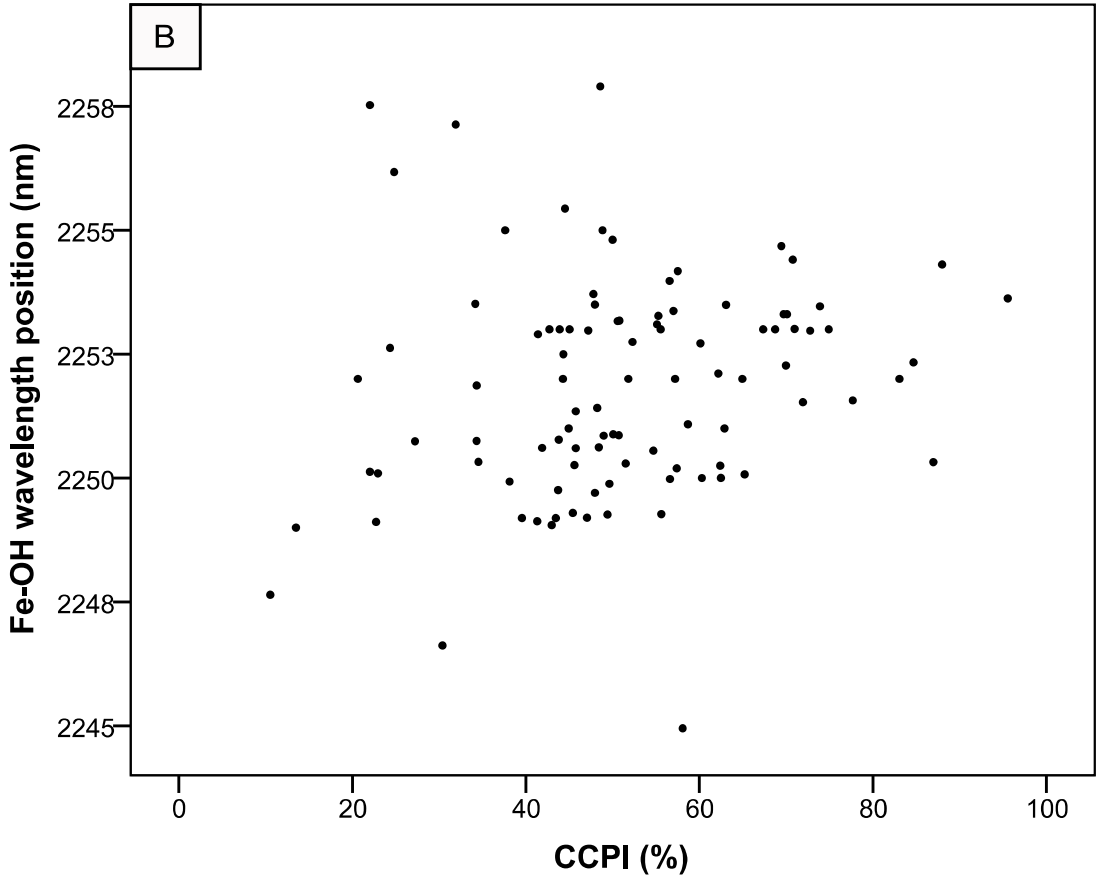
B
Fe-OH wavelength position (nm)
2258
2255
2253
2250
2248
2245
0
20
40
60
80
100
CCPI (%)

Figure 7

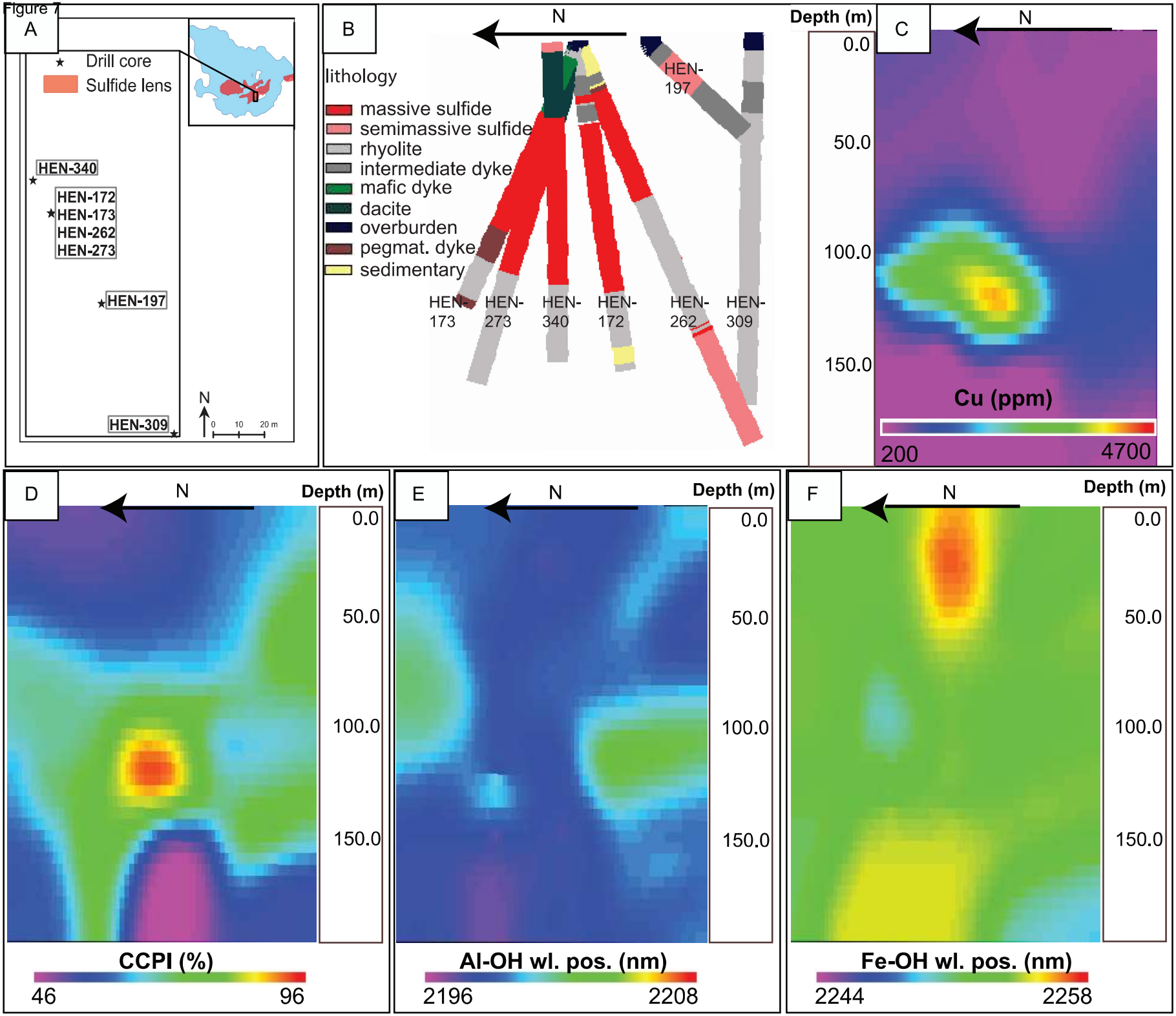
A
Drill core
Sulfide lens
HEN-340
HEN-172
HEN-173
HEN-262
HEN-273
HEN-197
HEN-309
N
0 10 20 m
B
N
lithology
massive sulfide
semimassive sulfide
rhyolite
intermediate dyke
mafic dyke
dacite
overburden
pegmat. dyke
sedimentary
HEN-197
HEN-173
HEN-273
HEN-340
HEN-172
HEN-262
HEN-309
Depth (m)
0.0
50.0
100.0
150.0
C
N
Cu (ppm)
200
4700
D
N
Depth (m)
0.0
50.0
100.0
150.0
CCPI (%)
46
96
E
N
Depth (m)
0.0
50.0
100.0
150.0
Al-OH wl. pos. (nm)
2196
2208
F
N
Depth (m)
0.0
50.0
100.0
150.0
Fe-OH wl. pos. (nm)
2244
2258

Figure 8

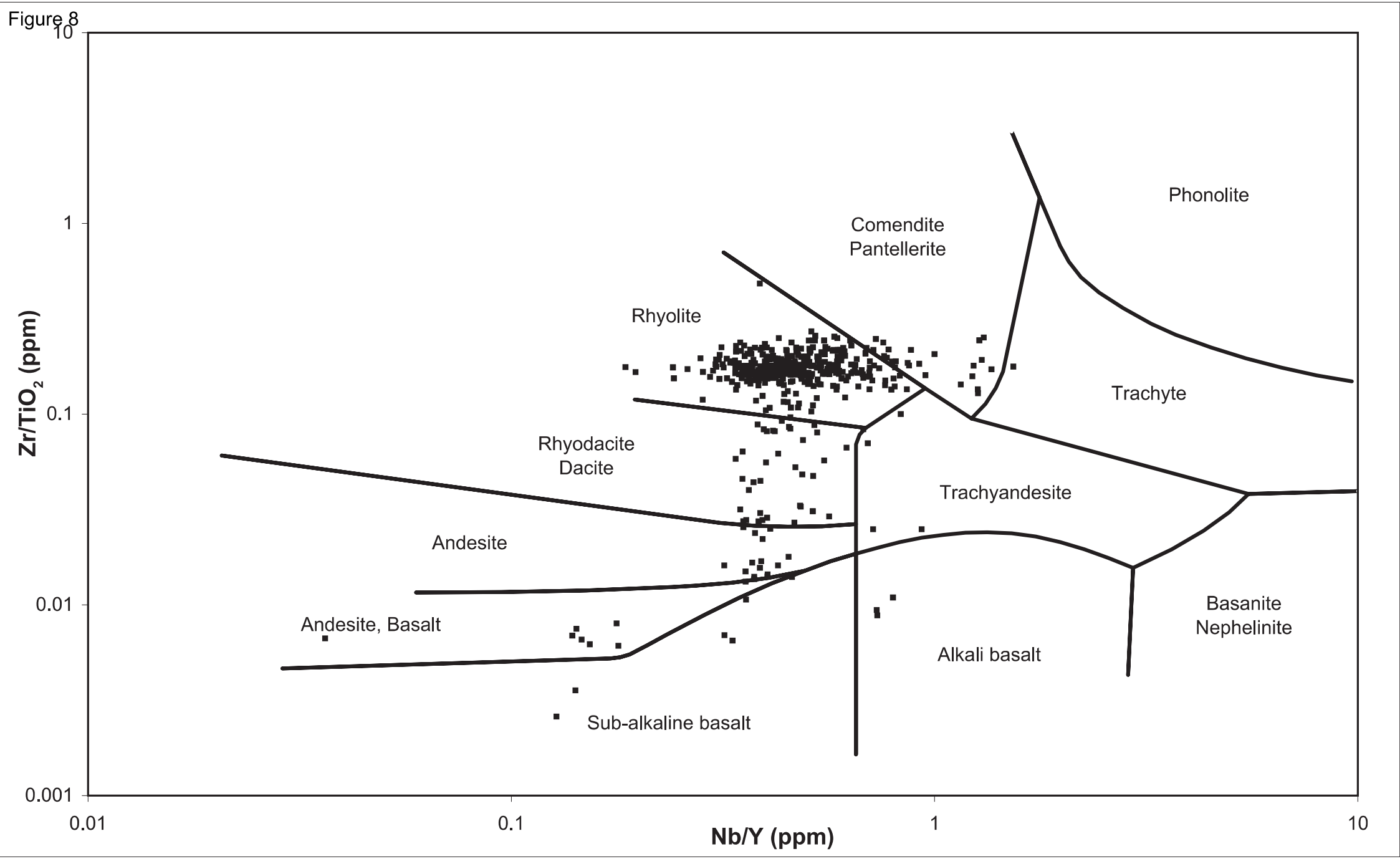
10
1
0.1
0.01
0.001
Zr/TiO2 (ppm)
0.01
0.1
1
10
Nb/Y (ppm)
Phonolite
Comendite
Pantellerite
Rhyolite
Trachyte
Rhyodacite
Dacite
Trachyandesite
Andesite
Andesite, Basalt
Basanite
Nephelinite
Alkali basalt
Sub-alkaline basalt

Figure 9

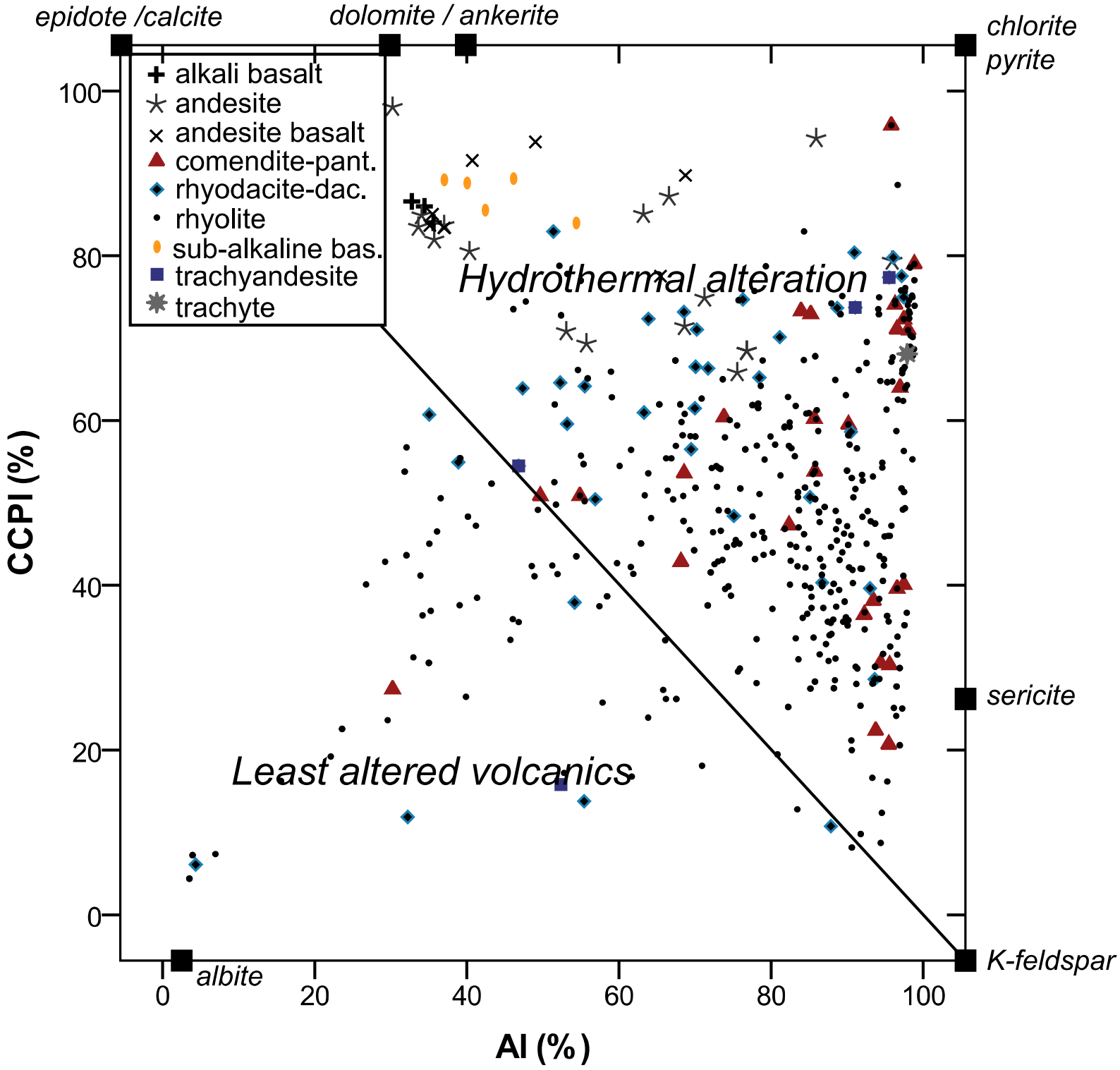
epidote /calcite
dolomite / ankerite
chlorite
pyrite
alkali basalt
andesite
andesite basalt
comendite-pant.
rhyodacite-dac.
rhyolite
sub-alkaline bas.
trachyandesite
trachyte
Hydrothermal alteration
Least altered volcanics
sericite
albite
K-feldspar
CCPI (%)
Al (%)
0
20
40
60
80
100

Figure 10

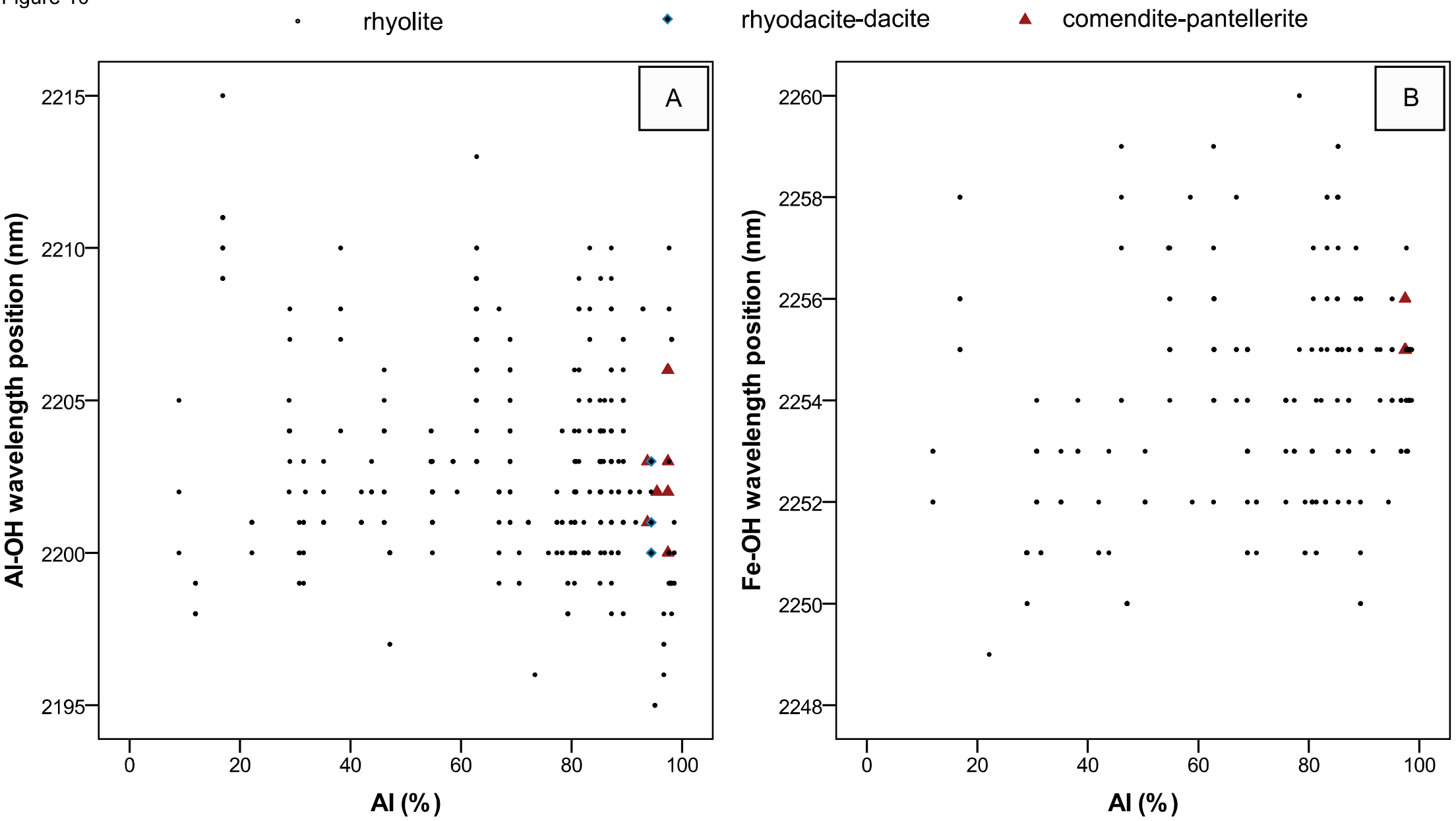
rhyolite
rhyodacite-dacite
comendite-pantellerite
A
B
Al-OH wavelength position (nm)
Fe-OH wavelength position (nm)
Al (%)
Al (%)
2215
2210
2205
2200
2195
2260
2258
2256
2254
2252
2250
2248
0
20
40
60
80
100

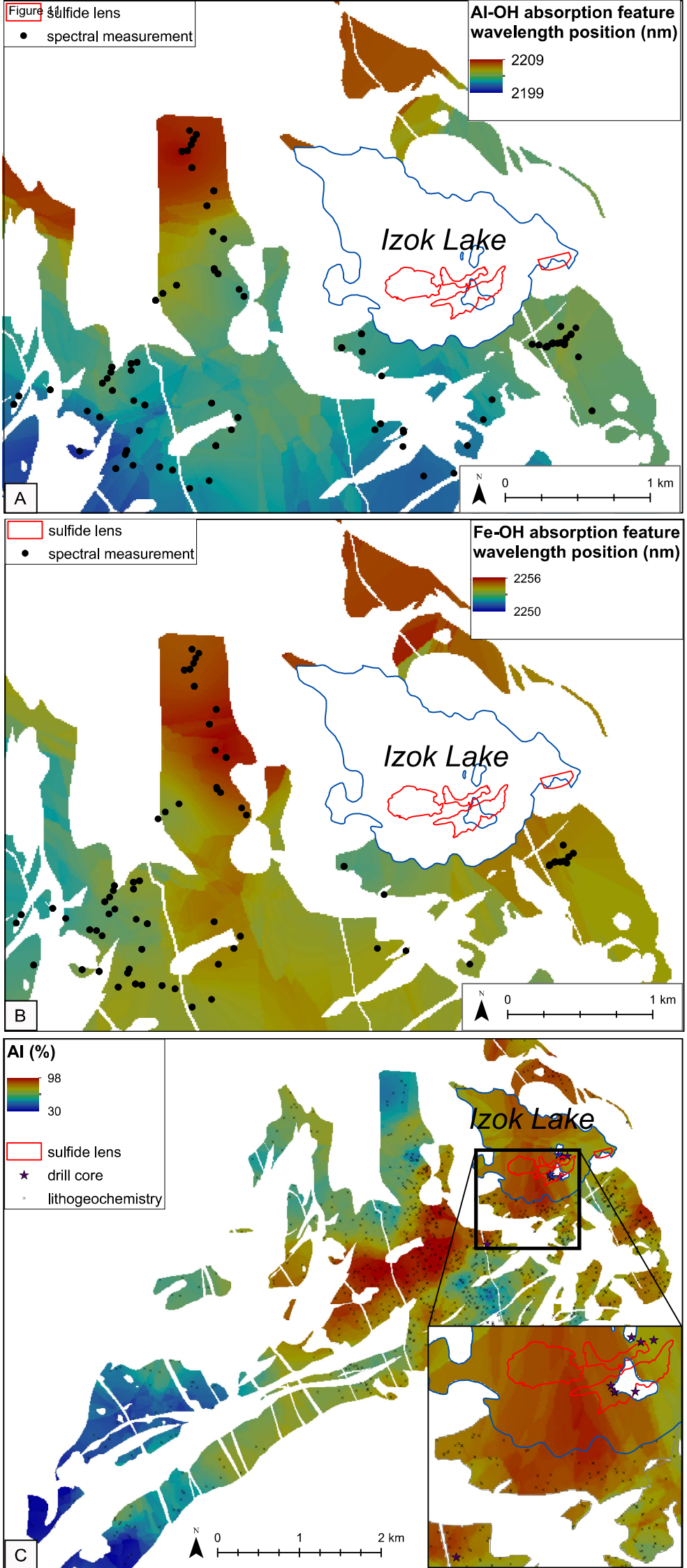
Figure 11
sulfide lens
spectral measurement
Al-OH absorption feature wavelength position (nm)
2209
2199
Izok Lake
N
0
1 km
A
sulfide lens
spectral measurement
Fe-OH absorption feature wavelength position (nm)
2256
2250
Izok Lake
N
0
1 km
B
Al (%)
98
30
sulfide lens
drill core
lithogeochemistry
Izok Lake
N
0
1
2 km
C

Figure 12

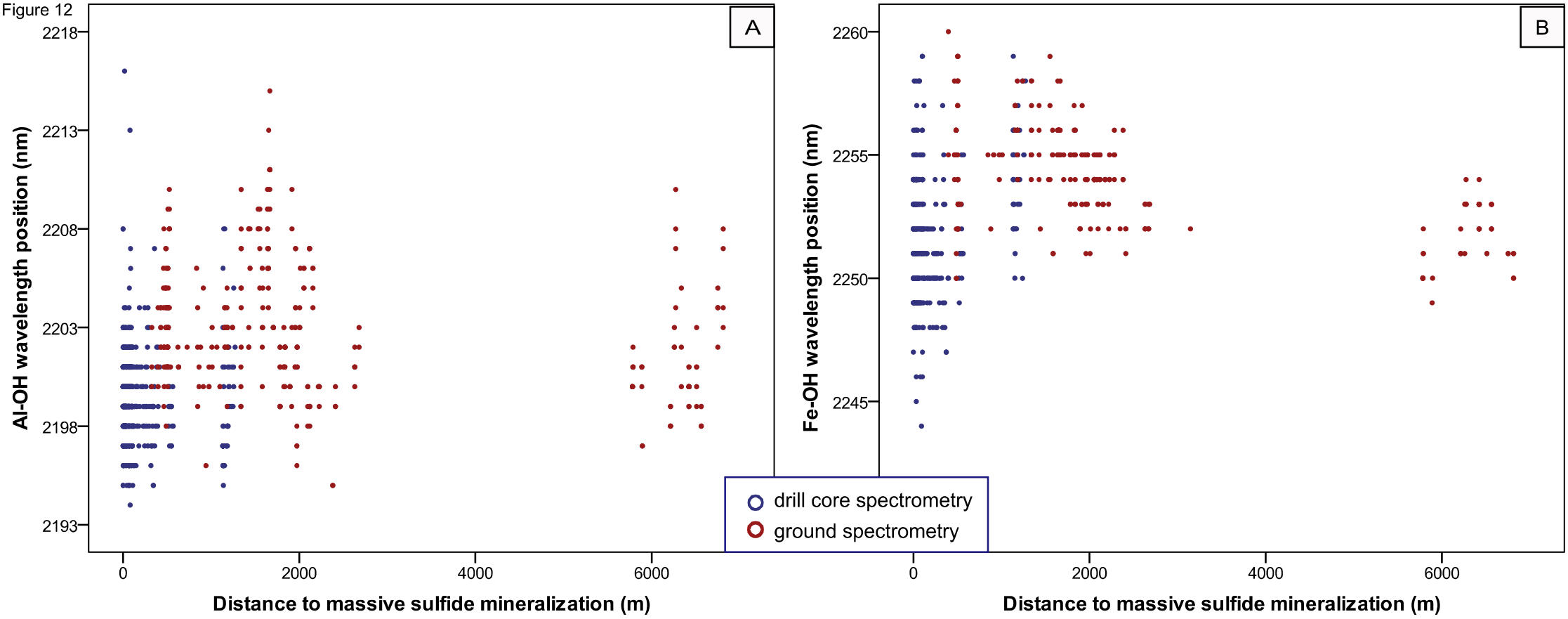
A
Al-OH wavelength position (nm)
2218
2213
2208
2203
2198
2193
0
2000
4000
6000
Distance to massive sulfide mineralization (m)
B
Fe-OH wavelength position (nm)
2260
2255
2250
2245
0
2000
4000
6000
Distance to massive sulfide mineralization (m)
drill core spectrometry
ground spectrometry

Table 1

	Min, nm	Max, nm	Median, nm	Mode, nm	Range, nm	*n*
Al-OH, ground spectrometry	2195	2215	2203	2203	21	357
Al-OH, drill core spectrometry	2194	2216	2199	2199	22	585
Fe-OH, ground spectrometry	2249	2260	2254	2255	12	264
Fe-OH, drill core spectrometry	2244	2259	2252	2250	15	344